

Influence of high-resolution wind forcing on hydrodynamic modeling of the Gulf of Lions

Amandine Schaeffer · Pierre Garreau · Anne Molcard ·
Philippe Fraunié · Yann Seity

Received: 21 October 2010 / Accepted: 13 May 2011 / Published online: 24 June 2011
© Springer-Verlag 2011

Abstract The impact of the choice of high-resolution atmospheric forcing on ocean summertime circulation in the Gulf of Lions (GoL; Mediterranean Sea) is evaluated using three different datasets: AROME (2.5 km, 1 h), ALADIN (9.5 km, 3 h), and MM5 (9 km, 3 h). A short-term ocean simulation covering a 3-month summer period was performed on a 400-m configuration of the GoL. The main regional features of both wind and oceanic dynamics were well-reproduced by all three atmospheric models. Yet, at smaller scales and for specific hydrodynamic processes, some differences became apparent. Inertial oscillations and mesoscale variability were accentuated when high-resolution forcing was used. Sensitivity tests suggest a predominant role for spatial rather than temporal resolution of wind. The determinant influence of wind stress curl was evidenced, both in the representation of a mesoscale eddy structure and in the generation of a specific upwelling cell in the north-western part of the gulf.

Keywords Coastal modeling · High resolution atmospheric forcing · Gulf of Lions · Wind stress curl · Upwelling

1 Introduction

The Gulf of Lions (GoL) is a large continental margin in the north-western Mediterranean Sea. Figure 1 shows its complex bathymetry, characterized by a shallow shelf (mean depth of 90 m), a complex coastline, and a shelf break dissected by numerous canyons. Like in most of the Mediterranean Sea, in this micro-tidal area, atmospheric forcing is a major driving component of coastal ocean dynamics. Prevailing winds originating from land, blowing offshore, also strongly influence GoL dynamics. Both northerly winds (Mistral) and northwesterly winds (Tramontane) are characterized by a strong channeling effect due to the marked land topography, leading to strong zonal wind gradients and shear close to the coast. These strong winds blow all year long, are cold in winter, and display a high temporal variability ranging from a few hours to a few days. Onshore winds from south/south-east are less frequent, usually slower and brief (less than three consecutive days). They can be extraordinarily strong and usually co-occur with rain and large swells.

Accordingly, the main hydrodynamic features of the GoL result from interactions with the atmosphere: summer up- and downwellings (Hua and Thomasset 1983; Millot 1979), inertial oscillations (Petrenko 2003; Millot and Crepon 1981), dense water formation and cascading in winter (Ulses et al. 2008; Herrmann et al. 2008; Béranger et al. 2010), and mesoscale eddy activity (Rubio et al. 2009a; Hu et al. 2009; Allou et al. 2010; Garreau et al. 2011).

In addition to atmospheric forcing, the circulation in the GoL is also influenced by freshwater input from the Rhône River (Ulses et al. 2005; Gatti et al. 2006) and the

Responsible Editor: Phil Peter Dyke

This article is part of the Topical Collection on *Joint Numerical Sea Modelling Group Workshop 2010*

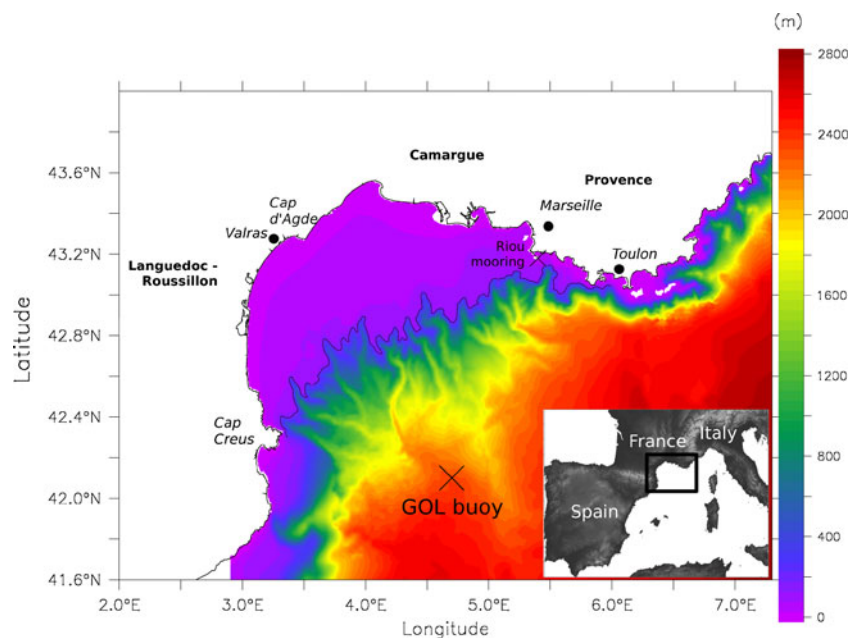
A. Schaeffer · A. Molcard · P. Fraunié
LSEET, Université du Sud Toulon-Var,
BP 20132, 83957 La Garde, France

A. Schaeffer (✉)
IFREMER, LER PAC,
BP 330, 83500 La Seyne sur Mer, France
e-mail: amandine.schaeffer@lseet.univ-tln.fr

P. Garreau
IFREMER, DYNECO/PHYSED,
BP 70, 29280 Plouzané, France

Y. Seity
Météo-France CNRM-GAME,
42 Av Gustave Coriolis,
31057 Toulouse Cedex, France

Fig. 1 Geographic map and model bathymetry of the GoL. The position of the meteorological buoy (GOL) and the Riou mooring are indicated and the gulf's southern delimitation (set to the 200 m isobath) is represented by the *black line*



bordering Northern Current (NC), which is the northern branch of the general circulation of the Mediterranean Sea (Millot and Wald 1980; Millot 1999). The NC displays large variability, with meandering sometimes intruding onto the shelf (Andre et al. 2009; Rubio et al. 2009b; Flexas et al. 2002).

Several modeling studies have investigated the influence of wind channeling on shelf circulation in this region, more specifically of the atmospheric forcing resolution on winter mixed layer depth, offshore dense water formation, and shelf convection or wave field description.

Using academic forcing in modeling experiments, Estournel et al. (2003) and Petrenko et al. (2008) investigated the impact of channeled or homogeneous northerly and northwesterly winds on the depth-averaged circulation during winter and stratified conditions, respectively. They evidenced completely different circulations at the gulf scale depending on the wind channeling. Moreover, the particular wind stress curl resulting from the conjunction of the Tramontane and the Mistral were found to lead the dominant winter circulation pattern: cyclonic circulation in the south-western part of the GOL and anticyclonic circulation in the eastern part.

In a long-term (10-year) simulation of the GoL, Langlais et al. (2009) compared the patterns of coastal dynamics using the REMO regional climate model (18 km, 1 h) or ERA40 global atmospheric reanalysis (125 km, 6 h). These authors confirmed the importance of regional channeling of the wind only represented in REMO forcing. At inter-annual to intra-seasonal time scales, they found similarities between the two atmospheric datasets, but the use of REMO with hourly sampling (instead of 6 h for ERA40)

enabled realistic reproduction of the thermal breeze systems and diurnal cycles observed in coastal waters. Moreover, with REMO, wind extremes were more numerous and significantly affected inertial oscillations and winter shelf dense water exportation through the canyons.

Focusing on inter-annual variability, Herrmann and Somot (2008) showed that “higher-resolution” atmospheric forcing (ERA40 downscaling of 50 km resolution compared with 125 km) was necessary to reproduce the observed oceanic winter convection located further offshore over the abyssal plain. They demonstrated the effect of enhanced spatial and temporal meteorological extremes.

Using 2.4 km atmospheric forcing, Lebeaupin-Brossier et al. (2009) investigated the impact of the air–sea coupling time frequency on the winter ocean mixed layer in the GoL. A time resolution of 3–6 h was shown to be too coarse to reproduce a fine-scale response of the ocean: internal ocean boundary layers as well as cooling and deepening of the ocean mixed layer under heavy precipitation events were not reproduced. Yet, atmospheric forcing at a 1-h time step appeared to be sufficient to satisfactorily reproduce extreme precipitation peaks and severe wind gusts.

Cavaleri and Bertotti (2004) explored the impact of different wind spatial resolutions of the ECMWF model on wind speeds and wave heights in semi-enclosed bays in the Mediterranean Sea. They concluded that a finer resolution improved the results: higher wind intensities, especially for onshore winds, and more realistic fetch lengths, which were also due to more precise topography.

In other regions, smaller-scale wind stress curl has been investigated thanks to progress in atmospheric model resolution. In the lee of the islands of Hawaii, using a

linear Ekman pumping model, Chavanne et al. (2002) and Yoshida et al. (2010) were able to relate mesoscale eddy generation to the local wind stress curl variability caused by the shattering effect of the island. Fennel and Lass (2007) analyzed changes in the upwelling of the Benguela system, alongshore and cross-shore currents caused by wind stress curls in coastal areas. Through analytical modeling, they evidenced complex dynamics resulting from cross-shelf variations in wind stress corresponding to specific regional features. In the California Current system, Pickett and Paduan (2003) showed local wind stress curl generated large local vertical velocities, providing a large proportion of upwelling transport through Ekman pumping.

More generally, Huthnance (2002) investigated the spatial and temporal details of the required wind forcing by considering various oceanic processes, including coastal trapped waves, upwellings and downwellings, stratification, sea breeze effects, coastal current, and plumes. He concluded that a wind field resolution of the order of 10 km or less, depending on the local orographic details, is required, with a temporal resolution of 1 to 3 h, especially to account for rapid and non-linear response.

Such spatial and temporal scales are now available for short-term simulations with even finer spatial resolutions of a few kilometers. Recently, a regional atmospheric model AROME was developed by the French met-office (Météo-France), with a spatial resolution of 2.5 km and hourly sampling. This model will soon be routinely available for atmospheric forecast operational oceanography and academic purposes.

AROME was already shown to significantly improve local weather prediction, such as forecasting local storms or intense precipitation (Boniface et al. 2009), as it includes sophisticated physics that accounts for short and intense processes. However, its usefulness in predicting coastal ocean circulation forcing remains to be investigated.

In the framework of operational oceanography, some wind forcings are available with a coarser resolution and

are commonly used to drive hydrodynamic modeling in the north-western Mediterranean Sea (<http://www.previmer.org>). Available wind forcings in this area are the ALADIN (9.5 km-3 h) atmospheric model from the Météo-France or a local built configuration of MM5 (9 km-3 h).

The aim of this paper is to evaluate the potential improvements expected in coastal modeling by AROME high-resolution forcing compared with ALADIN and MM5 and to characterize the relative influence of spatial versus temporal wind resolution. The study focuses on summer wind-driven hydrodynamic processes in the GoL, including upwellings, stratification, inertial oscillation, and small-scale eddy generation.

In the following section, we briefly describe the numerical meteorological and hydrodynamic models concerned. In Section 3, we compare and assess respective wind datasets via in situ observations to evaluate bias. In Section 4, we report our investigation of their impact on GoL dynamics in twin hydrodynamic modeling experiments using MARS3D (Model at Regional Scale, used in operational systems) and highlight some differences in specific ocean processes during summer. To focus on the impact of high-resolution wind forcing, additional simulations were performed using modified AROME fields, smoothed either over spatial or temporal resolution. In Section 5, we summarize and discuss our findings.

2 Specifications of numerical models

2.1 Weather forecast models: ALADIN, AROME, and MM5

Three distinct meteorological forcings were used to force twin hydrodynamic experiments. They differ in their physics, dynamics, assimilation system, and spatial and temporal resolutions. Table 1 summarizes some of the specifications described in this section.

Table 1 Characteristics of atmospheric models

MODEL	ALADIN France (Météo-France)	AROME (Météo-France)	MM5 (NCAR)
Horizontal mesh size	9.5 km	2.5 km	9 km
Number of vertical levels	60	41	26
Time output interval	3 h	1 h	3 h
Model providing LBC	ARPEGE(global)	ALADIN	NCEP GFS/MM5
mesh size	15 km for France	9.5 km	1° (~100 km)/27 km
time interval	3 h	1 h	6 h (3 h)
Type of data assimilation	3D-VAR	3D-VAR	None
Assimilation cycle	6 h	3 h	
SST used	Satellite	Satellite	Climatology

Both ALADIN (*Aire Limitée, Adaptation Dynamique, InterNational*, Fischer et al. 2005) and AROME weather forecasts models were developed by Météo-France.

ALADIN is a regional model widely used as meteorological forcing for Mediterranean hydrodynamic studies (Petrenko et al. 2005, 2008; Estournel et al. 2003, 2009; Dufois et al. 2008; Rubio et al. 2009a). Its horizontal mesh size is 9.5 km, with 60 vertical levels. It is a limited area version of the global ARPEGE/IFS model (*Action de Recherche Petite Echelle Grande Echelle* Courtier et al. 1994/Integrated Forecasting System). ALADIN is based on hydrostatic primitive equations, with a 6-h cycle 3D variational assimilation system.

AROME (*Application de la Recherche pour l'Opérationnel Méso-Echelle*) is the most recent Météo-France model, which has been run in a pre-operational way since December 2008 (Seity et al. 2011). It is a mesoscale model, with high spatial and output time resolution, 2.5 km and 1 h, respectively. Its dynamics derive from an ALADIN version without hydrostatic assumption (ALADIN-NH, Bubnova et al. 1995) while part of the physics is taken from Meso-NH model (Lafore et al. 1998). Deep convection is explicit, while shallow convection is parameterized using a mass flux scheme. A specific surface scheme SURFEX enables precise surface boundary conditions for turbulence and radiation terms. Some vertical levels are also inserted close to the surface thanks to a specific turbulent scheme (SBL, Masson and Seity 2009) allowing the prognostic calculation of 10 m wind, and 2 m temperature and humidity without analytical interpolation.

AROME's lateral boundary conditions and surface initial conditions are provided by ALADIN. Its data assimilation system is identical to the ALADIN 3D-Var scheme (Brousseau et al. 2008) except that it uses much sharper structure functions and a shorter 3-hourly assimilation cycle (rapid update cycle). The observations taken into account are the same as ALADIN's with similar spatial resolution, except for GPS Zenith Delays for which spatial observations are adapted to AROME's finer resolution. In addition, Doppler radars radial velocities from the French network are also assimilated.

MM5 (Mesoscale Model 5; Grell and Stauffer 1993) is another non-hydrostatic mesoscale model developed by the NCAR (National Center for Atmospheric Research). The configuration used in this study was built by ACRI ST (a private company), and derived from a nesting chain. Boundary and daily initial conditions were provided by the NCEP (National Centers for Environmental Prediction) GFS (Global Forecast System) model (spatial resolution of 1°). The nesting chain goes from a parent 27-km grid to a 9-km grid by two-way nesting. The output frequency is 3 h. No data assimilation is used in this nested configuration, but in the global GFS model providing daily initial

conditions. MM5 atmospheric forcing has been used in Mediterranean hydrodynamic simulations using the MARS3D model (Andre et al. 2005, 2009; Rubio et al. 2009b; Nicolle et al. 2009; Garreau et al. 2011) and is now routinely used in the operational forecast system Previmer (<http://www.previmer.org/en>).

2.2 Hydrodynamic model

Ocean simulations were performed using the primitive equation MARS3D model (Hydrodynamic Model for Application at Regional Scale) on a nested domain covering the GoL. Lazure and Dumas (2008) fully described the numerical model's specifications. It uses sigma coordinates and has the particularity of using a common time step to resolve the baroclinic and barotropic modes, based on the Alternating Direction Implicit scheme.

The regional configuration is centered on the GoL with a spatial resolution of 400 m and 30 uneven terrain-following levels discretizing the vertical direction, leading to vertical resolutions ranging from a few centimeters at the surface to 100 m at mid-water column for high depths. The initial condition and the lateral open-boundary fields are provided by the operational MENOR analyses (Nicolle et al. 2009), covering the north-western Mediterranean Sea with a horizontal mesh of 1,200 m. It is itself embedded in the global Mediterranean model of MOON (Mediterranean Operational Oceanography Network, Tonani et al. 2009; Pinardi et al. 2003) and forced by MM5 atmospheric forcing.

At lateral open boundaries, the forcing frequency is 3 h with a prescribed surface elevation (Dirichlet condition), while salinity and temperature fields are either clamped in the case of inflow or subjected to up-stream advection in the case of outflow. A zero-gradient condition is applied to baroclinic and barotropic velocities at open boundaries. Inside the domain, horizontal mixing coefficients derive from the Smagorinsky formula (Smagorinsky 1963) with a minimum set to 1 m²/s, increasing in a ten-cell-wide sponge layer (leading to a maximum value of 80 m²/s). Vertical turbulent coefficients are calculated with Pakanowski and Philander formulation tuned for the Mediterranean Sea (Pacanowski and Philander 1981), depending on the Richardson number.

The model bathymetry, shown in Fig. 1, was constructed using the 100-m resolution gridded file built by multibeam echosounder processing and available at Ifremer. Nine daily river outflows were considered, including the Rhône River which is divided into two mouths, the “Grand Rhône,” and the “Petit Rhône” and provides 90% of the terrestrial fresh water input (Ludwig et al. 2003).

In this study, the surface forcings were derived from each of the meteorological models previously presented,

providing wind components at a height of 10 m, temperature and relative humidity (at 2 m), precipitations, as well as longwave and shortwave radiative fluxes. Wind stress was calculated by MARS3D using a constant drag coefficient ($C_d=1.2 \cdot 10^{-3}$) in order to easily compare different forcing impacts. Turbulent heat fluxes (latent and sensible fluxes and evaporation) were deduced from Bulk formulae using the parametrization of Luyten and De Mulder 1992.

3 Evaluation and comparison of wind forcings

We compared the different atmospheric forcings described in the previous section (ALADIN, AROME, and MM5) and evaluated them using observations. Atmospheric forcing acts in different ways on the coastal ocean providing thermal and momentum flux. As this study is devoted to mesoscale dynamics, particular attention was paid to wind characteristics (strength, spatial and temporal variability) on the assumption that differences in thermal flux mainly affect regional scale bias.

A 3-month period was chosen, June to August 2008, as the strong summertime ocean stratification leads to marked

wind driven oceanic processes, such as upwelling, eddies, or inertial oscillations.

Two available observational datasets were used. First, daily QuikSCAT satellite measurements enabled a spatial description of the wind fields, with a coarse spatio-temporal resolution (1 day, $0.5^\circ \sim 50\text{km}$) compared with the different atmospheric models considered. An in situ meteorological buoy located in the southern GoL measures wind speed and direction every hour. This high frequency dataset enabled the wind extremes and temporal variability to be described very precisely.

3.1 Spatial variability

The Gulf of Lions is characterized by well-defined wind sectors, either continental winds channeled by the surrounding orography or oceanic winds. Figure 2 shows the mean 10-m wind vectors and the intensities derived from the atmospheric models and from QuikSCAT satellite observations for summer 2008. QuikSCAT gridded level 2B products provide daily ocean wind speed module and components with a spatial resolution of 0.5° (<http://cersat.ifremer.fr>, see Mean Wind Fields, User Manual, volume 2:

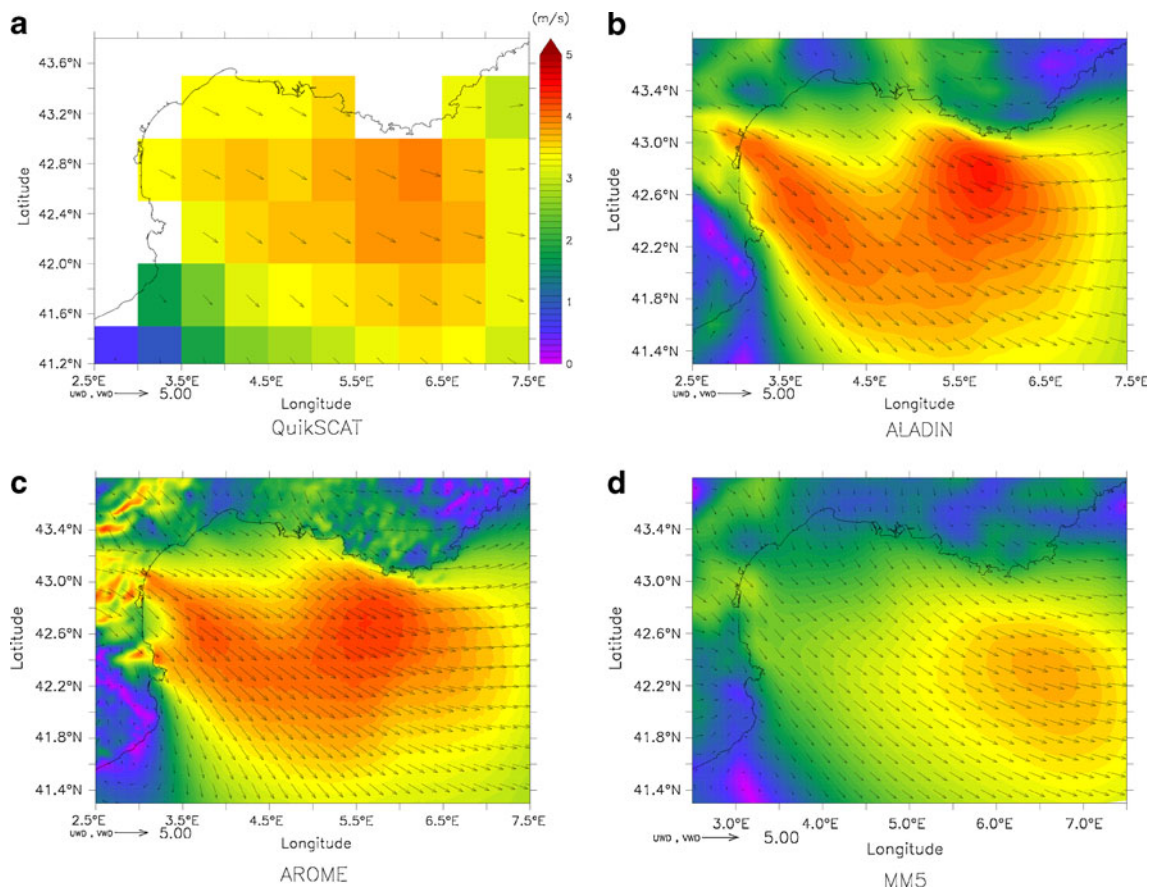


Fig. 2 Three-month averaged 10-m wind vectors and derived intensities (m/s) for summer 2008. **a** QuikSCAT data, **b** ALADIN, **c** AROME, and **d** MM5

QuikSCAT, 2002). In the Mediterranean Sea, these observations have already been checked using measurements made by meteorological buoys and compared with atmospheric models (Artale et al. 2010; Accadia et al. 2007; Ruti et al. 2008). The low spatial resolution with respect to the relatively small area of interest limits the analysis to a qualitative comparison.

The 2008 summer mean wind field was characterized by the occurrence of a northwesterly wind (Tramontane), channeled in the GoL and turning eastward in the eastern part of the area, following the coastline (Fig. 2). This wind direction was well-reproduced by all atmospheric models. Concerning intensities, AROME and ALADIN produced very similar patterns as the latter provided AROME's boundary conditions. They both simulated a strong wind patch on the gulf with a well-marked channeling effect on the northwestern part, this being a realistic feature given the adjacent land topography. The spatial resolution of QuikSCAT wind fields is not fine enough to represent such strong gradients. However, these satellite observations tended to confirm stronger intensities on the shelf than those modeled by MM5 which appeared to underestimate the strength of the Tramontane wind on the continental shelf.

Together with mean wind direction, wind stress curl has been shown to be a key parameter driving ocean dynamics, both in the open sea and on shallow shelves. In the GoL, Estournel et al. (2003) and Petrenko et al. (2005) concluded on the determinant influence of wind stress curl on depth-averaged circulations from ADCP data and modeling experiments. More recently, Garreau et al. (2011) highlighted the importance of the negative wind stress curl associated with the Tramontane on the generation of a mesoscale eddy in the south-western part of the shelf.

Figure 3 shows the time-averaged wind stress curl for summer 2008 provided by ALADIN, AROME, and MM5, respectively. Large-scale spatial distribution was similar with

each model and consistent with the dominant Tramontane: a positive curl on the eastern side of the GoL and a negative curl on the western side. However, both positive and negative rotational extrema were higher with AROME and ALADIN than with MM5, as highlighted in Fig. 3 with contour lines of $\pm 2.10^{-6} \text{ N/m}^3$ that are not present at all on MM5 mean fields. In fact, stress curl over the sea reached extrema that were 3.1 times higher with AROME than with ALADIN and 3.4 times with AROME than with MM5. Differences were particularly noticeable in the northern part of the gulf, where small features of positive curl were present with AROME, smoothed and lower with ALADIN and almost non-existent with MM5. In the higher-resolution AROME model, a more detailed coastline and orography also led to more localized patterns in the lee of Toulon islands (position shown on Fig. 1), close to the coastline and over land.

An empirical orthogonal function (EOF) analysis of the 3-month summer wind fields was performed to determine the dominant spatial patterns (not shown). First modes were similar in each meteorological model, corresponding to the major wind regimes of the region. The main differences concerned the number of modes needed to reach 90% of total variance, which was significantly higher with AROME at 20 compared with 9 and 6 with ALADIN and MM5, respectively. This suggests enhanced spatial variability in the AROME dataset, especially during summer when small-scale features such as thermal breezes are present. This was confirmed by instantaneous wind field images that exhibited more small spatial patterns and sharper fronts with AROME, while, with ALADIN and MM5, winds were smoother.

3.2 Wind intensity

In the area of interest, in situ measurements made by an offshore meteorological buoy are available. This GOL buoy

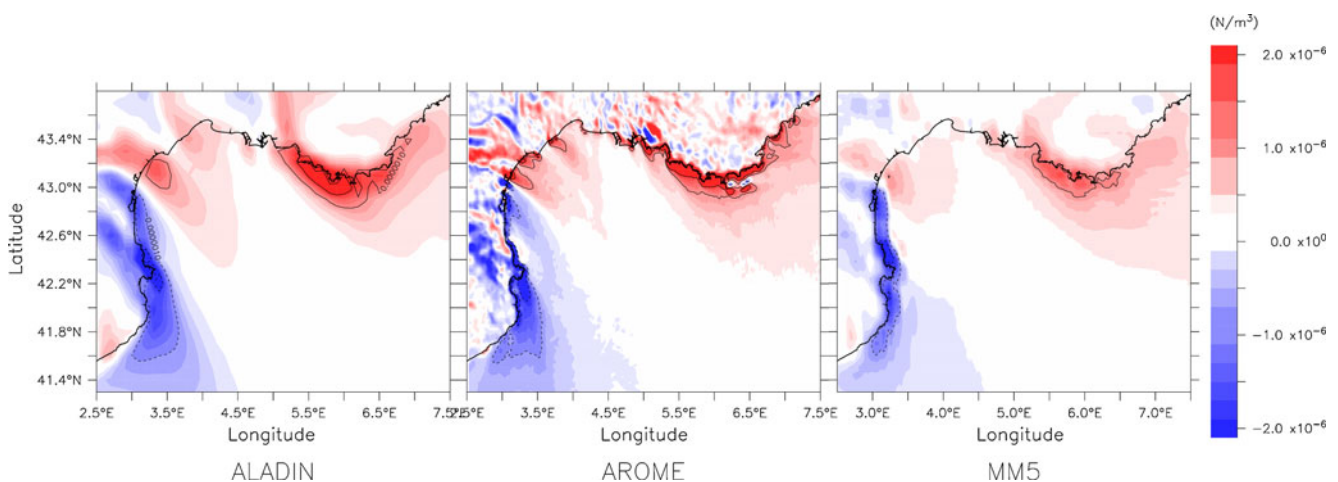


Fig. 3 Three-month averaged mean 10-m wind stress curl (N/m^3) for summer 2008 with the atmospheric models ALADIN, AROME, and MM5. Contours are -2.10^{-6} , -1.10^{-6} , 1.10^{-6} , and 2.10^{-6} N/m^3

is managed by Météo-France and positioned a few kilometers south of the continental shelf (4.7°E, 42.1°N), as shown in Fig. 1. It measures hourly air pressure at the surface, wind intensity and direction, air temperature, and relative humidity at a height of 3.60 m.

This high-quality dataset was used to evaluate the results of the atmospheric models from a statistical point of view. In situ wind intensities were multiplied by a factor of 1.1, obtained by the logarithmic wind profile law, to account for the different heights, as winds were modeled at a height of 10 m but measured at a height of 3.60 m. Ruti et al. (2008) compared this logarithmic method to the neutral stability correction method and evidenced similar errors, with a maximum bias of 0.5 m/s for strong winds.

Table 2 lists the statistical results of the modeled summer 2008 wind series compared with the in situ buoy measurements. As wind measurements for the 20 first days in June 2008 are missing, the comparison period is limited to mid-June until the end August 2008 for each wind component (west–east and south–north) and for wind speed. Mean values are presented for each dataset, together with mean bias error (model-observation), RMS error, and correlation coefficients comparing model results calculated at the location of the GOL buoy and measurements, with data series sampled at 1-h intervals.

The best model results for bias, RMS, and correlations were obtained for meridian wind components, which mainly reflect the oscillations between Mistral/Tramontane and southerly winds. The time-averaged values were negative, in accordance with the predominant Tramontane in summer 2008 (Fig. 2), while the high correlation rates indicated good reproduction of the North/South wind temporal variability by all atmospheric models.

The best overall agreements were obtained with the ALADIN dataset, with remarkable correlation factors (more than 0.93) and low RMS errors, whereas mean bias was lower with AROME. MM5 systematically displayed greater

differences with wind measurements at this buoy. It should be noted that the MM5 configuration has no data assimilation system, while both ALADIN and AROME assimilate some observations, including land station wind measurements and the surface pressure measured at the GOL buoy.

Another interesting particularity evidenced thanks to these wind comparisons was a systematic underestimation of wind speed for all components. The quantile–quantile plot in Fig. 4 focuses on wind intensity using the same datasets. In the figure, the distribution of modeled wind intensities is compared with measured values. The black line corresponding to a perfect fit is plotted as reference.

First, the figure reveals the inability of atmospheric models to reproduce wind extremes, as these are significantly underestimated. None of the models reproduced winds stronger than 18 m/s at the location of the buoy. Yet, these strong wind pulses are important for the ocean dynamics, as they provide considerable energy to the water mass. AROME and ALADIN showed a similar pattern, with better agreement in intensity distribution and values than MM5. Yet, over the whole domain, wind histograms revealed stronger winds in AROME fields (not shown). For instance, intensities higher than 8 m/s represented 3.6% of the wind fields with AROME in summer, 2.9% with ALADIN, and 1.4% with MM5.

4 Impact on hydrodynamic modeling

Atmospheric forcing is known to have a significant influence on hydrodynamic circulation, not only in surface layers but also at depth, especially in shallow gulfs. In the previous section, we reported that the atmospheric datasets were in good agreement concerning the summer large-scale wind pattern. Yet, they differed significantly when focusing on smaller-scale variability, like wind stress curl, which was

Table 2 Wind statistics at the GOL buoy (4.7°E, 42.1°N, position shown in Fig. 1. Bias, RMS, and correlation coefficients were calculated for each atmospheric model in comparison with buoy measurements

		BUOY	ALADIN	AROME	MM5
wind u-component	mean (m/s)	3.72	3.01	2.84	2.46
	bias (m/s)		−0.73	−0.95	−1.28
	RMS (m/s)		2,08	2,46	3,3
	correlation		0,96	0,86	0,74
wind v-component	mean (m/s)	−2.39	−2.1	−2.25	−1.58
	bias (m/s)		0.34	0.22	0.86
	RMS (m/s)		1.93	2.3	2.39
	correlation		0.95	0.92	0.93
wind intensity	mean (m/s)	7.34	6.08	6.4	5.77
	bias (m/s)		−1.26	−0.97	−1.56
	RMS (m/s)		2.22	2.47	3.03
	correlation		0.93	0.87	0.84

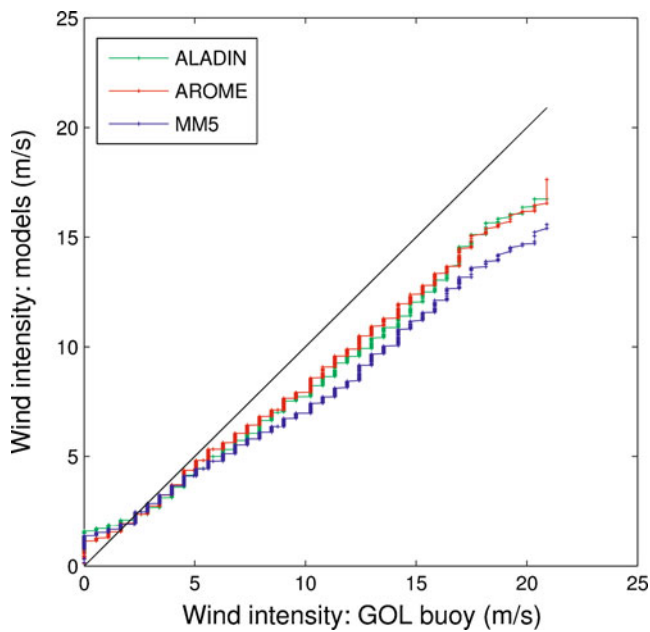


Fig. 4 Quantile–quantile plot of wind intensity (m/s), models versus in situ measurements for summer 2008 at GOL buoy with ALADIN in green, AROME in red, and MM5 in blue

enhanced in AROME fields, or extreme event intensities, which were particularly underestimated with MM5. In this section, we evaluate the differences in the hydrodynamic circulation resulting from the choice of meteorological forcing.

Twin ocean simulations were run for the same summer period. Each atmospheric model dataset was used individually to force a high-resolution hydrodynamic model, using the same bulk parameterization for each simulation.

In addition to the three distinct meteorological forcings, sensitivity tests were performed by reducing the variability of the AROME dataset, as shown in Table 3. This experiment enabled us to identify and differentiate the influence of the high spatial and temporal resolution. “AROME3h” refers to a lower temporal resolution at 3 h compared with 1 h for the original AROME outputs. “AROME10km” stands for a coarser spatial resolution:

10 km compared with 2.5 km in the original dataset. In order to assess exclusively wind small-scale variability, “AROMEeof” has the same original resolution (1 h, 2.5 km). However, wind fields were reconstructed using the 20 first EOF modes, representing 90% of total variance. In other words, it corresponds to a smoothed version of the original wind fields that respects mean velocities.

The choice of atmospheric forcings did not influence large-scale hydrodynamic circulation, which was similar whatever dataset used. Indeed, even a 9-km and 3-h resolution was sufficient to reproduce realistic patterns, like diurnal cycles or the distinction between Mistral and Tramontane winds that are needed for realistic depth-integrated circulation, as highlighted by Estoumel et al. (2003). In the following section, the impact of the wind on the GoL dynamics is analyzed in terms of stratification, upwelling systems, inertial oscillations, and mesoscale variability.

4.1 SST and stratification

First, satellite data were used to validate sea surface temperature (SST). SST NAR products were from NOAA/AVHRR, with a spatial resolution of 0.1° (~ 10 km). Statistics were calculated for night conditions (at 2 AM for observations and 3 AM for model outputs) to avoid overheating of a skin surface layer in the case of calm sunny weather. Only locations where satellite coverage reaches at least 25% of the whole period were taken into account.

For most of the GoL, the mean bias was quite low using ALADIN or AROME, with errors barely exceeding 0.5°C . Using MM5 atmospheric forcing led to overestimation of the surface temperature of between 0.5°C and 1°C over the stratified part of the gulf. This can be imputed to a lower wind stress inducing less evaporation, latent heat flux, and vertical mixing, as radiative solar and long-wave heat fluxes remained similar with each meteorological forcing. Nevertheless, in the north-eastern part of the area, the surface temperature was clearly too low compared with satellite data, independently of the meteorological forcing. This can be imputed to the lack of small-scale variability in

Table 3 Sensitivity tests of AROME model for wind field, temperature, relative humidity, surface pressure, radiative thermal fluxes and precipitations

Differences compared with AROME fields	Wind field (10 m) m/s	T, RH (2 m) $^\circ\text{C}$, /	Pressure (surface) hPa	Radiative fluxes long and short wave W/m^2	Precipitations kg/m^2
AROME3h	3-h instantaneous	3-h instantaneous	3-h instantaneous	3-h instantaneous	3-h instantaneous
AROME10km	10-km truncated	10-km truncated	10-km truncated	10-km truncated	10-km truncated
AROMEeof	Reconstitution with 20 first EOF modes (90% of total variance)	Unchanged	Unchanged	Unchanged	Unchanged

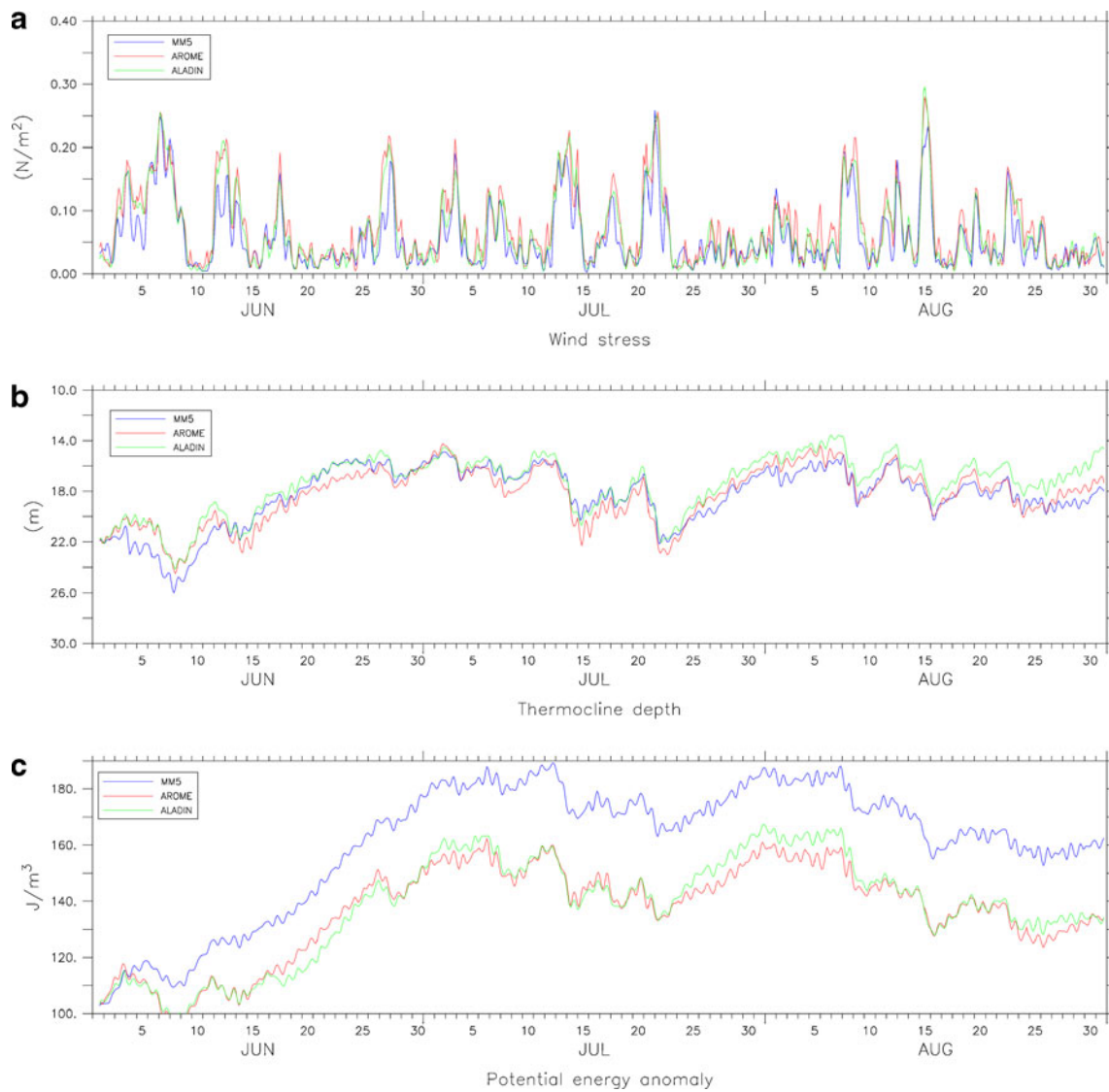


Fig. 5 Changes in **a** mean wind stress (N/m^2), **b** mean thermocline depth (m), **c** potential energy anomaly (J/m^3) over time for summer 2008. Values are spatially averaged over the gulf (depth <200m, area of averaging shown in Fig. 1)

ocean modeling that could modify simulation of the frontal dynamics and accelerate the relaxation of upwelling systems, for instance, see below in upwelling discussion. Figure 5 shows summer stratification at the scale of the gulf, with the mean depth of the thermocline (defined as the depth of the maximum vertical temperature gradient). The mean thermocline depth barely depended on the data forcing used and was strongly linked to variations in wind stress. The thermocline was situated between 15 and 25 m in depth, in accordance with climatology for summer conditions, and deepened in response to a strong wind event, for instance, on June 8 or July 22, 2008.

A more detailed diagnosis of stratification, the potential energy anomaly (PEA), enabled us to highlight some

differences resulting from the choice of the meteorological forcing used. PEA was defined by Simpson and Bowers (1981) as:

$$\varphi = \frac{1}{D} \int_{-H}^{\eta} gz(\rho - \bar{\rho})dz$$

Where ρ and $\bar{\rho}$ are respectively the local and depth-averaged density, and D is the total depth (being the sum of mean depth H and surface elevation η). The PEA represents the amount of mechanical energy (per volume unit) required to instantaneously homogenize the water column with a given density stratification. Hence, the lower the PEA, the more homogeneous the water column, and a

higher value could indicate regions with strong stratification. The PEA appears to be a powerful criterion to study mixing through wind and tide stirring (De Boer et al. 2008) or stratification resulting from surface heating or river discharge (Burchard and Hofmeister 2008).

In Fig. 5, the PEA is spatially averaged over the gulf for summer 2008. Using MM5 atmospheric forcing, the water column was more stable in summer, which is consistent with a warmer surface layer. The impact of lower wind stress can be assumed. The fact that MM5 underestimated wind did not notably modify the depth of the thermocline but increased the stability of the water column.

4.2 Upwellings

Upwellings are of great importance for biogeochemical issues as they act directly on vertical mixing along coasts, as well as on horizontal dispersion through extending filaments. Furthermore, they are a direct consequence of wind stress, through wind intensity and direction. Millot (1979, 1990) listed six different cells commonly observed by satellite data in the GoL, which appear during continental winds (Mistral or Tramontane). Using a two-

layer model, Hua and Thomasset (1983) were able to relate the different cell locations to the specific geometry of the coastline. The upwelling cells in the eastern and the northern GoL were shown to be the consequence of the favorable direction of the Mistral and the Tramontane, respectively. When the general direction of the wind is not favorable for upwelling (like the Tramontane in the north-western part of the GoL, since it blows perpendicular to the general coastline), these authors assume that locally some correctly oriented short coastline segments may produce strong and localized upwelling. In the western part of the GoL, the coastline discontinuity at the Cap d'Agde (Fig. 1) has been said to be the main factor responsible for upwelling during the Tramontane in this area. Nevertheless, as already shown by Millot (1979), secondary upwelling may also occur along this coast with no obviously favorable segment (off Sète or Valras for instance). Since, in this part of the GoL, the atmospheric models exhibited differences in the mean wind stress curl (Fig. 3), we investigated their potential effect on local upwelling.

Figure 6a shows the locations of the modeled upwellings as a function of the meteorological forcing considered, by representing the fifth percentile of surface temperature over

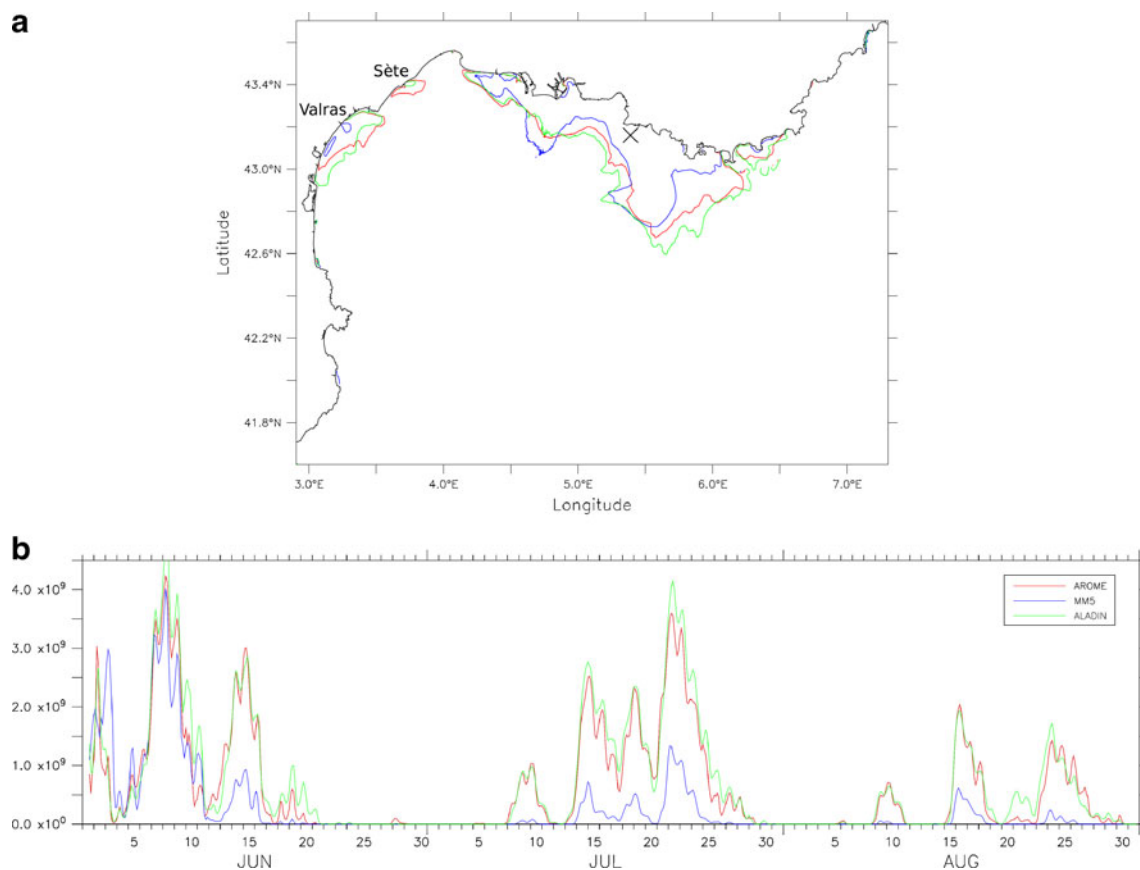


Fig. 6 **a** Spatial extension of surface temperature percentile05: contour of iso-17.5°C. **b**. Changes in upwelling area (m²) over time for summer 2008, defined as SST < 17.5°C. Hydrodynamic model

results using ALADIN atmospheric forcing are in *green*, using AROME in *red*, and using MM5 in *blue*

the summer 2008. This corresponds to the time average of the 5% lowest SST values for each grid point. The 17.5°C contour is shown because it appears to be a good indicator of unstratified conditions in this region (see Fig. 7). It satisfactorily represents the persistent locations of upwellings in accordance with the map of Millot (1979). On the eastern coast of the GoL where the upwelling is a consequence of north-westerly winds blowing parallel to the coast, all atmospheric forcings generated upwelling. The offshore extension was only reduced when MM5 forcing was used, as winds were less intense and blew less parallel to the coast, as shown in Fig. 2. On the north-western coast of the GoL, the use of different wind forcings led to different upwelling patterns. Our configuration of MM5 forcing did not result in notable cooling of the sea surface temperature in this area. Upwelling cells on the north-western coast near Valras and Sète appeared with AROME. ALADIN wind forcing only showed an upwelling near Valras.

Changes in the upwelling surface are plotted in Fig. 6b, showing good agreement in time between wind forcings for most episodes, but, again, the spatial surface of low SST value (< 17.5°C), representing the upwelling expansion,

was much smaller using MM5 meteorological forcing. In early June, when the stratification was weak and the Mistral was dominant, the three available forcings were almost in agreement. In July and August, the effect of MM5 forcing on SST was clearly weaker.

To enable these differences to be evaluated, Fig. 7 compares modeled temperatures to in situ measurements collected in the framework of the Medchange project (<http://medchange.org>) at RIOU mooring, close to Marseille where upwelling is expected (black cross in Fig. 6). The mooring comprises eight sensors uniformly distributed from 5 to 40 m in depth and records changes in temperature at hourly intervals. Measured temperature profiles (top panel of Fig. 7) showed clear upwelling events corresponding to the rapid rise of cold water to the surface. For instance, on July 4, the temperature at a depth of 5 m decreased by 6°C in 18 h. Modeled upwelling events using AROME and ALADIN were in good agreement with in situ data, both in terms of the time of the occurrence of upwellings and the duration, whereas they were underestimated with MM5. With MM5, some events were either shorter showing less surface cooling (June 15, July 16) or

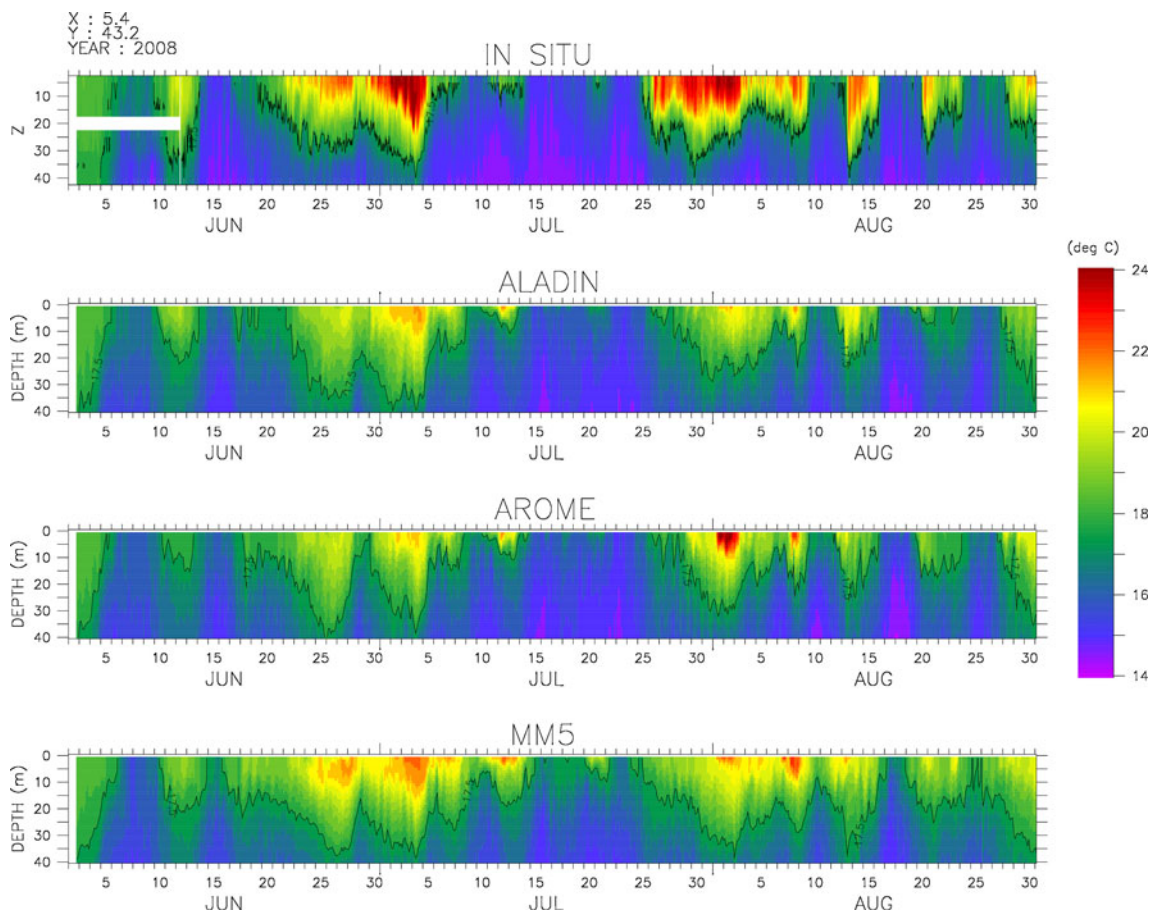


Fig. 7 Hovmuller temperature diagram (°C) at RIOU mooring (5.4°E, 43.2°N): from *top to lower panel*: in situ measurements, model results using ALADIN, AROME, and MM5. 17.5°C-isotherm is superimposed

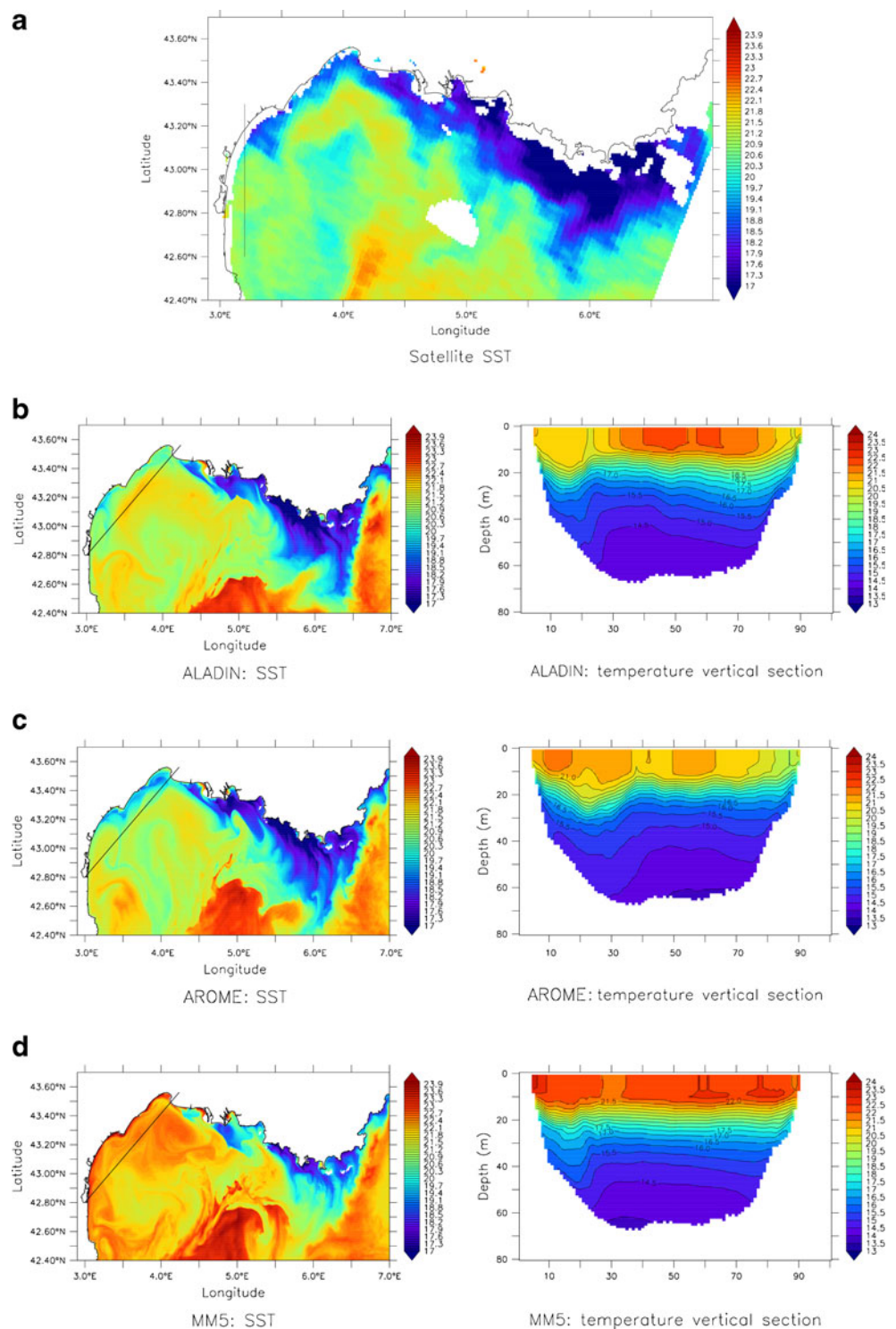
entirely missing (August 25). It should be noted that none of the simulations correctly reproduced the observed reheating of SST. In late June and early July, the two observed successive reheatings were progressive in both numerical modeling and in situ observations. Reheating needs about 5 days to recreate a surface mixed layer and a thermocline. In such cases, an improvement can be expected from a better evaluation of the heat flux at the surface or from a more sophisticated scheme for the evaluation of vertical fluxes. In late July and in August, the observed reheating after an upwelling event was very sudden indicating an advection of warm water, whereas, in the models, events were progressive, suggesting that a vertical process dominated. The dynamics of the upwelling relaxation was inadequately simulated. This was probably either a consequence of the lack of small-scale wind features or the lack of a sub-mesoscale structure in the oceanic frontal dynamics, such as instabilities, filaments, meanders, or vertical turbulence that could increase horizontal mixing and favor relaxation of the upwelling as shown by Rousset et al. (2009) in the case of a re-stratification after a convection event.

To enable assessment of upwelling cells and spatial extension, Fig. 8 compares SST images from satellite AVHRR data and model results on July 10, 2008. This date was chosen for the quality of satellite data and the evidence of upwelling cells. Again, the cooling of SST on the eastern coast was well-represented using AROME or ALADIN and underestimated using MM5 meteorological forcing. With AROME forcing, the frontal zone exhibited more very small-scale instabilities generating filaments. On the north-western coast, the Valras upwelling is present on the satellite image, including an elongated feature resembling a southward filament, associated with a patch of warmer water in the south (3.25° E, 42.9° N). Hua and Thomasset (1983) suggested that the elongation of the upwelling was associated with an anticyclonic eddy in the western part of the GoL. However, they were not able to reproduce such a feature through their idealized modeling and pointed out the lack of spatial and temporal variability in the applied wind stress. Hu et al. (2009) modeled a large anticyclonic structure in the western part of the GoL using ALADIN atmospheric forcing and different diffusion setups to reproduce the structure of chlorophyll concentration revealed by the satellite. In the present study, the warmer patch observed in the SST was smaller than the one in Hu et al. (2009) but well-reproduced with AROME forcing. According to the model velocities, it corresponded to an anticyclonic eddy, not shown with MM5, where the Valras upwelling was also missing. A cross-section parallel to the north-western coast representing the temperature is also shown in the Fig. 8 for each meteorological forcing. With MM5 wind forcing, the mixed surface layer was nearly

homogeneous and constant in thickness. Both ALADIN and AROME forcing generated variations in depth and in temperature for the surface layer. A contribution of wind stress curl and Ekman pumping is suggested. Figure 9a shows changes in wind stress curl over time in July 2008 on a section at longitude 3.2° E (latitude 42.6° to 43.3° N), resulting from the different atmospheric models. The wind vectors are also superimposed at latitude 43° N. The lower panel shows the corresponding changes in surface temperature and currents. Using AROME or ALADIN forcing, upwellings formed near the coast (3.2° E, 43.2° N) during northwesterly winds (Tramontane; e.g., 8–9, 15–16, 18–19, 22–23 July). According to the configuration of the local coastline, these winds are oriented in a cross-shelf direction. While the wind orientation modeled by MM5 was similar for some events (see the wind vector in Fig. 9a), wind stress curl values were much lower due to the spatially smoothed structure shown in Fig. 3. With AROME and ALADIN local wind, fields corresponding to Tramontane were characterized by a delimitation between positive curl (in red) in the north and a negative curl in the south (in blue), with values around $4\text{--}6 \cdot 10^{-6} \text{N/m}^3$. Looking at surface currents, anticyclonic circulation developing south of the upwellings can be observed, for instance on July 18–20.

The influence of wind stress curl on upwelling systems has already been demonstrated. In addition to coastal upwellings due to Ekman transport when wind blows alongshore, curl-driven upwellings could also arise through Ekman pumping. In that case, wind stress curl causes a divergence (positive curl) at the sea surface (Gill 1982). Ekman pumping is well-known in the open ocean but has also been evidenced in coastal areas. Pickett and Paduan (2003) concluded that these two processes were equally important in generating some upwellings in the Californian Current system, i.e., close to local promontories responsible for wind stress curl. In Baja California, winter “Santa Ana” winds blow from land through local mountains, producing offshore jets with intense wind-stress curl on both sides. Trasvina et al. (2003) found good agreement between Ekman pumping velocity and the alternate warm and cold areas along the coast. They concluded that the formation of upwellings was caused by offshore channeled winds. In the Gulf of Tehuantepec, Mexico, similar upwelling filaments were observed and were attributed to the curl of the land wind stress. They were associated with a mesoscale anticyclonic eddy on the right flank of the wind track and sometimes with a short-living cyclonic structure on the left flank (Trasviña et al. 1995; Barton et al. (1993); Trasvina and Barton 2008). Crepon and Richez (1982) developed the analytical solution for the linear Ekman theory for offshore wind forcing, perpendicular to the coast. They evidenced the formation of a dipole structure in the upper layer. According to McCreary et al. (1989), the response can be

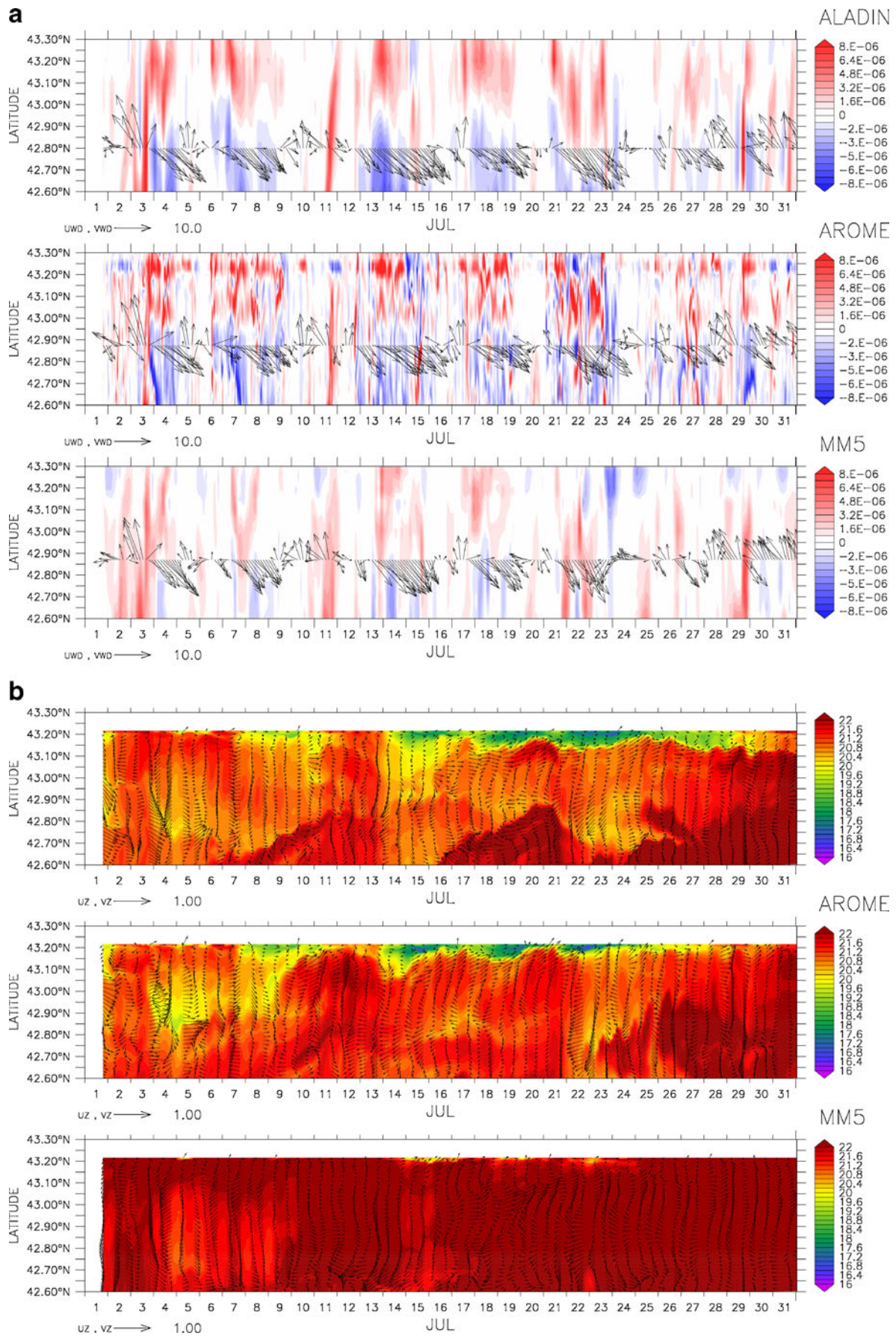
Fig. 8 **a** Satellite SST image (°C) on July 10, 2008 (AVHRR/NOAA), the transect for Fig. 9 is superimposed. **b–d** Corresponding model SST (same color bar) and vertical temperature profiles from the transects represented in the *left panels* (°C). **b** simulations with ALADIN, **c** with AROME, **d** with MM5



asymmetrical with a dominating anticyclone, especially when the thermocline is shallow because Ekman suction is then limited.

In the configuration in the western GoL, the Tramontane wind exhibits high gradients since it is strongly channeled by the land topography, leading to a zero-curl line separating rather high curl values (Figs. 3 and 9a). To

assess the link between the wind curl, the Valras upwelling, and the anticyclonic structure in the GoL, an idealized numerical experiment was conducted with MARS3D, respecting the observed orders of magnitude. The configuration was simplified with a straight coastline, a vertical density profile that was homogeneous in the horizontal direction, and a cross-shore wind. The bathymetry and



stratification were similar to those in the GoL in July 2008 (Fig. 10a), with a shallow gulf with a maximum depth of 200 m and a thermocline localized at a depth of around 20 m. The applied wind had a positive curl on the eastern side and an opposite symmetric negative curl on the western side, with extreme values of $\pm 4.10^{-6} \text{ N/m}^3$ and jet width corresponding to the Tramontane configuration of the observed upwelling (150 km). No heat fluxes were taken into account, and the wind forcing was kept constant for 3 days.

Through Ekman pumping, a divergence appeared on the positive curl side, together with a convergence on the negative curl side, clearly perceptible in the temperature section (Fig. 10b). In this academic experiment, the variation in the thickness and in the temperature of the surface layer was in agreement with the results found with AROME and ALADIN in a realistic situation (Fig. 8b, c). Figure 10c shows the resulting surface temperature and currents after 3 days of wind forcing, indicating a surface cooling of 0.5°C . In the meantime, an anticyclonic eddy was generated close to the coast, strongly enhanced by adjacent water pumping. Its diameter was about 40 km, consistent with the structure observed in the south-western GoL (Fig. 8c). The eddy length scale appeared to be correlated with wind curl rather than with stratification, as the local internal Rossby deformation radius was low given the stratification ($\sim 5 \text{ km}$). In accordance with McCreary et al. (1989), the circulation was asymmetric, and no cyclonic structure was formed on the other flank. Therefore, the channeling of the Tramontane significantly contributed to the upwelling processes in the north-western part of the GoL. The smoothed pattern of MM5 forcing was not able to cause significant upwelling in this area.

4.3 Inertial oscillations

In stratified conditions, internal wave generation in the coastal ocean is often associated with a transitory geostrophic adjustment at the coastline in response to wind pulse. In that case, wind stress can be spatially homogeneous (Tintore et al. 1995; Davies and Xing 2004). By inducing horizontal variations of Ekman suction, the wind stress curl can also lead to the formation of near-inertial waves far from the coast, the most famous example being traveling storms (Gill 1984). Internal inertial oscillations were observed in both in situ measurements and in simulations. In the following section, we report investigations of the effect of the spatial and temporal resolution of wind forcing.

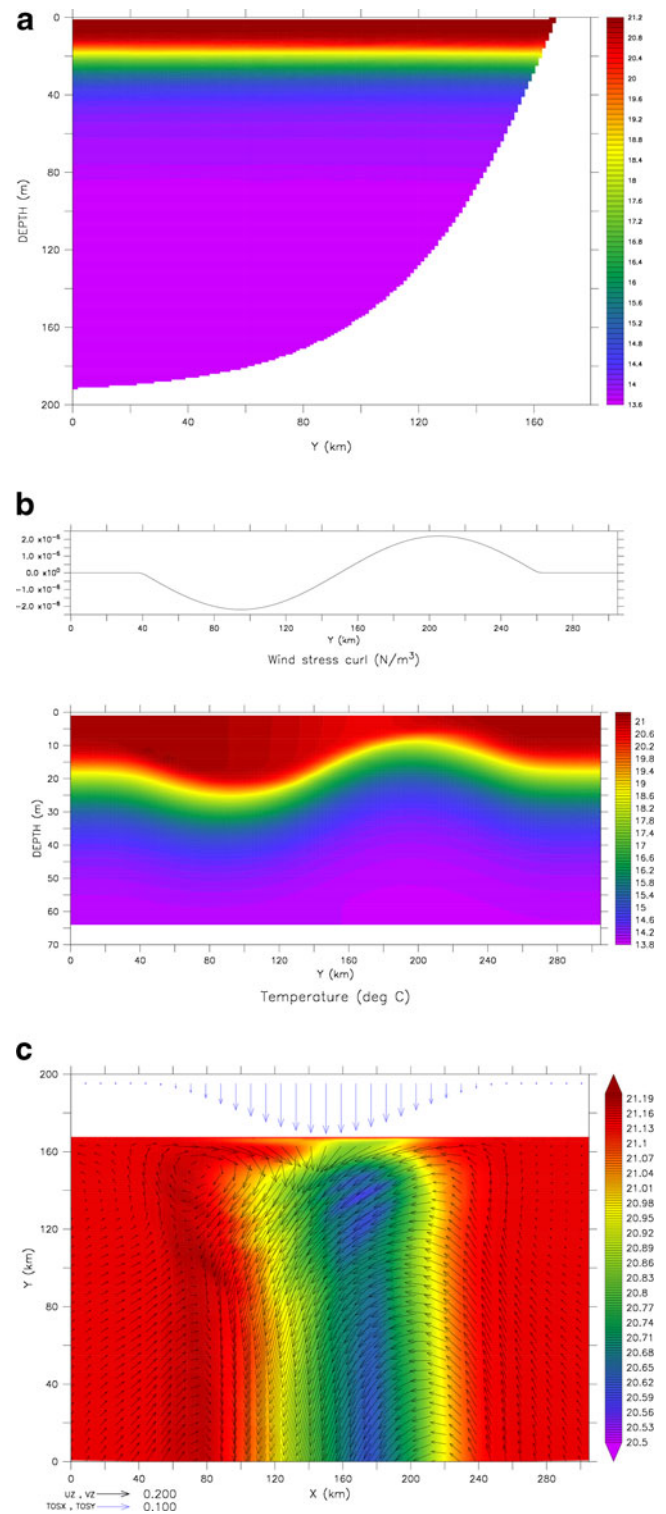


Fig. 10 Idealized numerical simulation. **a** Initial temperature section ($^\circ\text{C}$) and bathymetry. **b** Wind stress curl section (*upper panel*) and temperature section at $y=150 \text{ km}$ resulting from 3 days of constant wind (*lower panel*). **c** Surface temperature ($^\circ\text{C}$) and current vectors (m/s), after 3 days of wind stress represented by *blue arrows* (wind stress is constant in y -direction)

◀ **Fig. 9** Changes over time at section (3.2°E , $42.6\text{--}43.3^\circ\text{N}$) in **a** wind stress curl using the different atmospheric models (ALADIN, AROME, and MM5). Wind vectors at 43°N are superimposed. **b** Corresponding sea surface temperature ($^\circ\text{C}$) and current vectors (m/s)

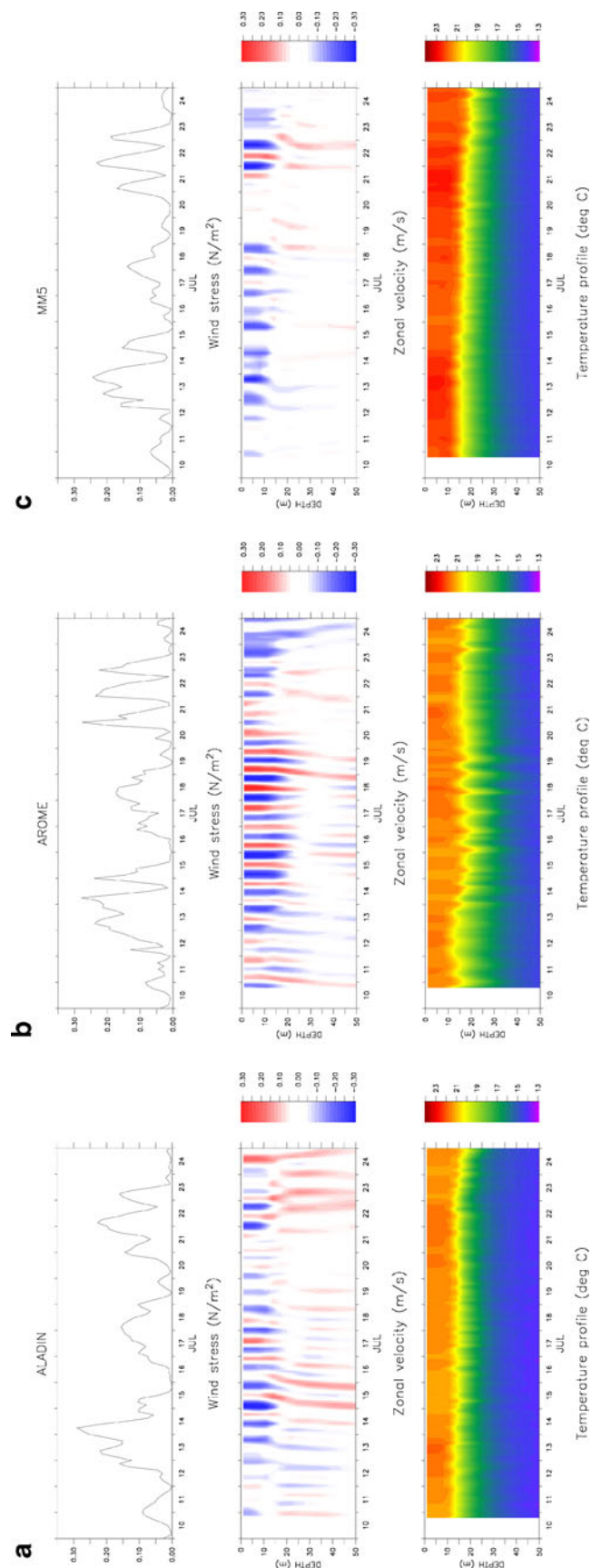
In the GoL, inertial oscillations have been observed many times in stratified conditions using ADCP current measurements and temperature profiles (Millot and Crepon 1981; Petrenko 2003; Petrenko et al. 2008). In particular, Millot and Crepon (1981) showed that inertial currents were 180° out of phase between the surface and the bottom layer, with thermocline vertical displacements up to 10–20 m high. They were able to reproduce these features using a two-layer analytical model with a uniform impulsively started cross-shore wind.

The thermocline oscillation associated with inertial waves is visible in the Hovmuller diagram of temperature profiles. Figure 11 shows changes in temperature and the zonal velocities vertical profiles in the middle of the gulf (4°E , 43°N) over time in July 2008 as a function of the atmospheric forcing used. Using AROME, the thermocline vertical displacement reached amplitudes of 10 m at the quasi-inertial frequency (17.5 h at the GoL latitudes). Associated zonal velocities also exhibited inertial oscillations with an out-of-phase direction between the upper and lower layers, for instance, on July 15, 2008. The corresponding wind forcing exhibited strong pulses. Using ALADIN or MM5, both thermocline and current oscillations were weaker. This was confirmed by a more quantitative analysis: the power spectral density of temperature summer time series versus depth is shown in Fig. 12, which compares results obtained with the three atmospheric datasets. For each simulation and depth, a spectral analysis of the July temperature time series was computed, and the amplitudes corresponding to inertial and diurnal frequency were extracted.

Solid lines represent signals at diurnal frequency; dashed lines correspond to quasi-inertial frequency. For each meteorological forcing, the diurnal signal of temperature was strong at the surface, mainly due to solar heat fluxes, and decreased with depth. Conversely, inertial signals were maximum around the thermocline at a depth of 20 m, with an amplitude of about 0.2°C using AROME, much weaker with ALADIN, and even lower with MM5. The sensitivity tests using AROME atmospheric fields (AROME3h, AROME10km, and AROMEeof) enabled us to link these differences with the wind field resolution. The high spatial resolution appears to be determinant for the enhancement of inertial oscillation (Fig. 12b). Indeed, while a temporal resolution reduced to 3 h did not significantly affect the inertial signal, spatial smoothing applied either on spatial resolution (AROME10km) or on small-scale variability (AROMEeof) led to weaker wind pulses and curls, and thus to smaller inertial oscillations.

4.4 Mesoscale variability

At mesoscale, Pujol and Larnicol (2005) and Jordi and Wang (2009) studied spatial variability in the Mediterra-



◀ **Fig. 11** Changes in wind stress (N/m²), zonal velocity profile (m/s), and temperature profile (°C) over time in July 2008 at (4°E,43°N). From *left to right*: using ALADIN, AROME, and MM5

nean basins, using eddy kinetic energy (EKE) derived from merged altimetric data. In the western basin, they evidenced permanent or recurrent structures especially in the Alboran Sea and along the Algerian coasts. However, in the GoL, altimetric data resolution (14 km, weekly maps) is too coarse to detect small scale variability, as the internal Rossby deformation radius is around 7–10 km (calculated from MEDAR-MEDATLAS climatologies).

Here, the EKE per unit mass was computed from the numerical simulations to compare the impact of forcing on mesoscale activity. The eddy kinetic energy appeared to be highly dependent on atmospheric forcing, as shown in Table 4. The model EKE was computed by averaging summer values, as follows:

$$EKE = \frac{1}{2} \left((u - \bar{u})^2 + (v - \bar{v})^2 \right),$$

where u and v are the instantaneous zonal and meridional current velocities, integrated over the 0–50-m surface layer, and \bar{u} , \bar{v} are the monthly means. EKE values are averaged over the summer and spatially over the gulf. Overall, higher values were obtained with AROME meteorological forcing than with ALADIN and MM5 (Table 4). Sensitivity experiments on the reduction of AROME resolution for summer enhanced the impact of wind variability which was smoothed in the AROMEof experiment, leading to weaker local wind intensity and curl, and consequently to lower eddy variability.

The mean EKE values were high, as a consequence of several intense eddy structures, especially an anticyclonic eddy that continued for several weeks in June 2008. Figure 13 shows images of the Okubo-Weiss parameter at a depth of 20 m and velocity vectors at different dates, and shows changes in this anticyclonic structure off Creus Cape. The Okubo-Weiss parameter W enabled vorticity and strain in an eddy field to be highlighted (Isern-fontanet et al. 2004):

$$W = \left(\frac{\partial u}{\partial x} - \frac{\partial v}{\partial y} \right)^2 + \left(\frac{\partial v}{\partial x} + \frac{\partial u}{\partial y} \right)^2 - \left(\frac{\partial v}{\partial x} - \frac{\partial u}{\partial y} \right)^2$$

A main eddy was positioned in the western part of the gulf (3.2°E, 42°N), with a vertical extent of ~100 m, a horizontal diameter of between 25 and 40 km, intensities reaching 0.3–0.4 m/s at the surface, and thermohaline characteristics (low-density core) corresponding to the eddy studied by Rubio et al. (2005) and Rubio et al. (2009a). Its generation mechanism was linked to intense northwesterly wind conditions, driving a coastal southward flow that separates downstream from Creus Cape. Model results confirmed this generation mechanism but revealed marked changes in the eddy over time, depending on the atmospheric forcing used. Figure 13 compares model results with satellite images: chlorophyll-a concentration from MODIS products and sea surface temperature from AVHRR/NOAA. The dates were chosen for the significant eddy signature on one or both of the in situ observations. On June 5, a patch of warm water with high chlorophyll concentration water was clearly visible off Creus Cape. This anticyclonic eddy was observed at the same location in 20-m depth currents, at a similar intensity and size using all

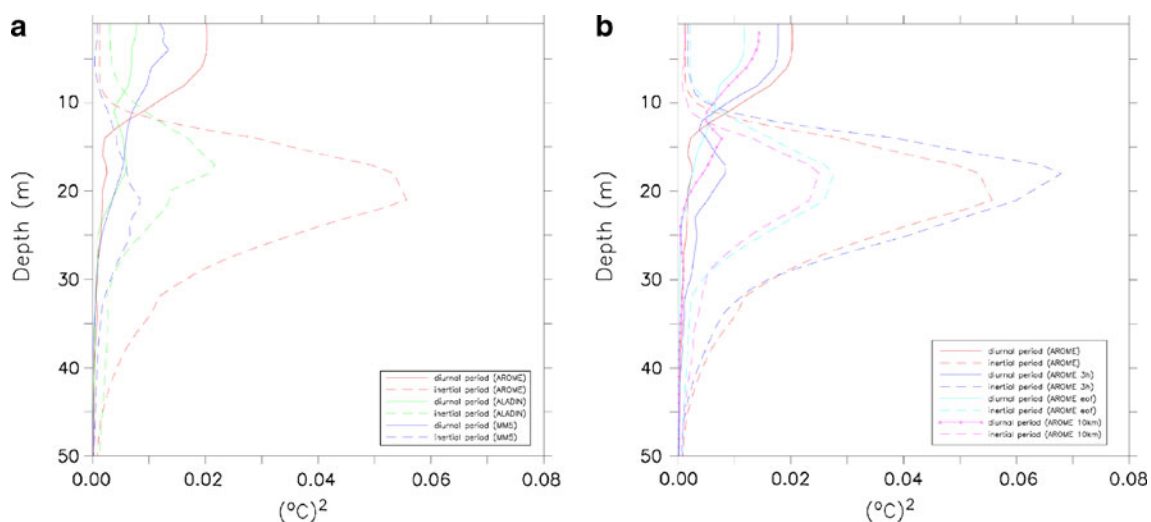


Fig. 12 Power spectral density of temperature time series (°C²) versus depth for July 2008 at (4°E, 43°N). *Solid lines* represent diurnal frequency, *dashed lines* quasi-inertial frequency. **a** Simulations with

ALADIN, AROME, or MM5 atmospheric forcings. **b** Sensitivity tests on the AROME dataset: simulations with AROME, AROME3h, AROME10km, and AROMEof

Table 4 Monthly eddy kinetic energy per unit mass for summer 2008, averaged over the gulf (depth < 200 m, area of averaging shown in Fig. 1)

Atmospheric forcing	ALADIN	MM5	AROME	AROME3h	AROME10km	AROMEeof
Mean eddy kinetic energy (m ² /s ²)	0.0059	0.0049	0.0068	0.0068	0.0067	0.0061

atmospheric forcings. The eddy was advected southward over a period of 1 month with all datasets except AROME and AROME3h. Finally, using AROME, on July 5, the anticyclonic structure moved to the Catalan shelf, which was confirmed by the simultaneous SST image, while with other forcings it disappeared from the area. Garreau et al. (2011) were able to link the intensification of such an eddy to the negative wind stress curl of the Tramontane, carrying less dense water from the Catalan Sea to the western gulf, thus providing more available potential energy for the structure. This is consistent with our results, as AROME fields displayed more stress curl in the area (Fig. 3) than ALADIN and MM5. In addition, the similar behavior of AROME and AROME3h compared with AROME10km and AROMEeof confirmed the dominance of spatial variability over temporal variability in changes in the structure.

5 Conclusion

The present study was designed to investigate the sensitivity of GoL hydrodynamics to high-resolution atmospheric forcing. Indeed, operational atmospheric models are currently available with high resolutions, both in space and time, and can be used to model coastal oceanic forcing.

The new operational forecasting model AROME (2.5 km, 1 h) developed by Météo-France was analyzed by comparing it with the former ALADIN (9.5 km, 3 h) and NCAR-MM5 models (9 km, 3 h) for wind forcing of coastal flows in the north-western Mediterranean Sea. In addition, sensitivity experiments were performed on the original AROME dataset by reducing its spatial resolution, time sampling, or wind small-scale variability. All these datasets were then used independently to force a 400-m hydrodynamic configuration of the GoL. Several wind-driven summer ocean processes were analyzed, compared with real observations when available, and related to atmospheric forcing and its resolution.

In comparison with temperature mooring measurements and satellite observations, upwelling events and spatial expansion in the eastern part of the GoL were better reproduced by AROME and ALADIN than by MM5, which underestimated wind intensities in summer 2008. This underestimation can be corrected using Bulk formula with an adapted drag coefficient.

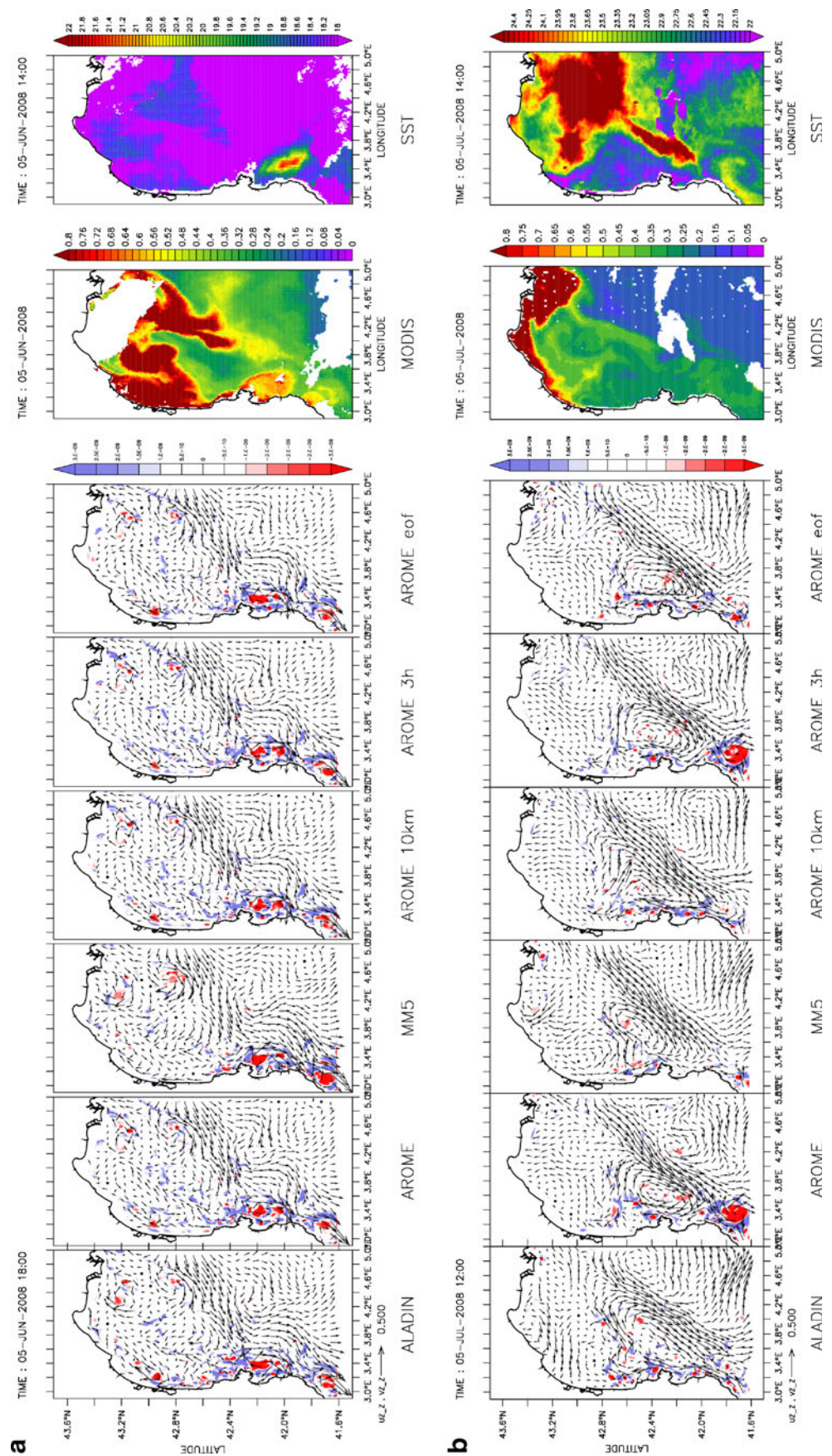
However, the simulation with MM5 also failed to capture the Cap d'Agde upwelling and the adjacent anticyclonic structure. We suggest that formation of the upwelling is linked to the local wind curl rather than to Ekman transport from alongshore wind stress. Indeed, this upwelling is generated during offshore Tramontane winds, which are characterized by a strong channeling effect. Through Ekman pumping, a divergence of surface layers occurs on the positive curl side, leading to a well-defined upwelling. Then, an anticyclonic eddy is generated on the negative curl side, enhanced by the adjacent warm water advection at the surface. This eddy advects cold upwelled waters and generates a filament skirting around it. Similar wind curl-generated upwellings with an associated asymmetric circulation have already been evidenced in other areas (near the Californian and Mexican coasts). An idealized numerical experiment respecting the regional orders of magnitude confirmed this assumption.

The influence of wind stress curl was also evidenced on the generation and intensification of a mesoscale structure in the western part of the Gol by Garreau et al. (2011). During summer 2008, a similar anticyclonic eddy structure was captured by the hydrodynamic simulations and its evolution assessed through SST or chlorophyll-a observations. Only the ocean model driven by AROME based on 1-h or 3-h sampling succeeded in representing its survival time on the shelf. This can be explained by the fact that stronger negative curls are present in AROME wind fields when a high spatial resolution is used, favoring the transport of warm Catalan water to the shelf and providing available potential energy.

Actually, this study showed the relevance of spatial variability in different processes. Spatial smoothing of AROME atmospheric forcing led to lower inertial oscillations and energetic variability, while temporal smoothing did not affect ocean response. Such vertical movements of the thermocline or an increase in the depth of the mixed layer caused by an eddy structure are expected to have considerable influence on bio-geochemical processes.

Consequently, a higher spatial resolution (2.5 km) appears to be an improvement, while using a temporal resolution finer than 3 h for the atmospheric resolution is not necessary. While bulk parameterization can be adapted and optimized for each atmospheric forcing, the spatial variability of wind fields depends exclusively on the atmospheric model when only one-way coupling is considered.

Fig. 13 Simulated 20-m deep currents and Okubo-Weiss parameter (s^{-2}) as a function of the atmospheric forcing used (ALADIN, AROME, MM5, AROME10km, AROME3h, AROMEeof), corresponding satellite images of MODIS chlorophyll-a concentration and AVHRR/NOAA SST. **a** June 5, 2008, **b** July 5, 2008



Ultimately, two-way coupling including feedback on ocean response in atmospheric fields will undoubtedly be required for finer resolutions, as wind stress is also affected by the ocean, via SST, especially when upwellings are present (Jin et al. 2009; Chelton et al. 2007).

The available AROME forcing was too short (only 3 months in summer) to enable definitive conclusions to be made about improvements achieved by atmospheric modeling in operational oceanography. Nevertheless, we demonstrated that the small spatial scales present in the meteorological field can modify both the mesoscale and the general dynamics of the GoL. Consequently, having a correct high-resolution meteorological model helps derive the intense eddy activity observed in the GoL in a more deterministic way.

Acknowledgments The research was supported by IFREMER and Météo-France in the framework of a PhD grant and by GIRAC *Pôle Mer* project. The authors would like to thank ACRI ST for managing the MM5 configuration and gratefully acknowledge the Medchange program and, in particular, Nathaniel Bensoussan for providing the Riou temperature time series. Most of the simulations were run using IFREMER computation facilities.

References

- Accadia C, Zecchetto S, Lavagnini A, Speranza A (2007) Comparison of 10-m wind forecasts from a regional area model and QuikSCAT Scatterometer wind observations over the Mediterranean Sea. *Mon Weather Rev* 135:1945–1960
- Allou A, Forget P, Devenon JL (2010) Submesoscale vortex structures at the entrance of the Gulf of Lions in the Northwestern Mediterranean Sea. *Cont Shelf Res* 30(7):724–732
- Andre G, Garreau P, Garnier V, Fraunie P (2005) Modelled variability of the sea surface circulation in the North Western Mediterranean Sea and in the Gulf of Lions. *Ocean Dyn* 55:294–308
- Andre G, Garreau P, Fraunie P (2009) Mesoscale slope current variability in the Gulf of Lions. Interpretation of in situ measurements using a three dimensional model. *Cont Shelf Res* 29(2):407–423
- Artale V, Calmanti S, Carillo A, Dell'Aquila A, Herrmann M, Pisacane G, Ruti P, Sannino G, Struglia M, Giorgi F, Bi X, Pal J, Rauscher S (2010) An atmosphere–ocean regional climate model for the Mediterranean area: assessment of a present climate simulation. *Climate Dyn* 35:721–740
- Barton ED, Argote ML, Brown J, Kosro PM, Lavin M, Robles JM, Smith RL, Trasviña A, Velez HS (1993) Supersquirt: dynamics of the Gulf of Tehuantepec, Mexico. *Oceanography* 6:23–30
- Béranger K, Drillet Y, Houssais MN, Testor P, Bourdallé-Badie R, Alhammoud B, Bozec A, Mortier L, Bouruet-Aubertot P, Crépon M (2010) Impact of the spatial distribution of the atmospheric forcing on water mass formation in the Mediterranean Sea. *J Geophys Res* 115:C12041
- Boniface K, Ducrocq V, Jaubert G, Yan X, Brousseau P, Masson F, Champollion C, Chery J, Doerflinger E (2009) Impact of high-resolution data assimilation of GPS zenith delay on Mediterranean heavy rainfall forecasting. *Ann Geophys* 27(7):2739–2753
- Brousseau P, Bouttier F, Hello G, Seity Y, Fischer C, Berre L, Montmerle T, Auger L, Malardel S (2008) A prototype convective-scale data assimilation system for operation: the Arome-RUC. HIRLAM Tech Rep 68:23–30
- Bubnova R, Hello G, Benard P, Geleyn J (1995) Integration of the fully elastic equations cast in the hydrostatic-pressure terrain-following coordinate in the framework of the ARPEGE/Aladin nwp system. *Mon Weather Rev* 123(2):515–535
- Burchard H, Hofmeister R (2008) A dynamic equation for the potential energy anomaly for analysing mixing and stratification in estuaries and coastal seas. *Estuar Coast Shelf Sci* 77(4):679–687
- Cavaleri L, Bertotti L (2004) Accuracy of the modelled wind and wave fields in enclosed seas. *Tellus* 56a:167–175
- Chavanne C, Flament P, Lumpkin R, Dousset B, Bentamy A (2002) Scatterometer observations of wind variations induced by oceanic islands: implications for wind-driven ocean circulation. *Can J Remote Sens* 28:466–474
- Chelton DB, Schlax MG, Samelson RM (2007) Summertime coupling between sea surface temperature and wind stress in the California Current System. *J Phys Oceanogr* 37(3):495–517
- Courtier P, Thepaut J, Hollingsworth A (1994) A strategy for operational implementation of 4D-VAR, using an incremental approach. *Q J R Meteorol Soc* 120:1367–1387
- Crepon M, Richez C (1982) Transient upwelling generated by two-dimensional atmospheric forcing and variability in the coastline. *J Phys Oceanogr* 12:14371457
- Davies A, Xing J (2004) Modelling processes influencing wind-induced internal wave generation and propagation. *Cont Shelf Res* 24(18):2245–2271
- De Boer GJ, Pietrzak JD, Winterwerp JC (2008) Using the potential energy anomaly equation to investigate tidal straining and advection of stratification in a region of freshwater influence. *Ocean Model* 22(1–2):1–11
- Dufois F, Garreau P, Le Hir P, Forget P (2008) Wave- and current-induced bottom shear stress distribution in the Gulf of Lions. *Cont Shelf Res* 28:1920–1934
- Estoumel C, Durrieu DeMadron X, Marsaleix P, Auclair F, Julliard C, Vehil R (2003) Observation and modelisation of the winter coastal oceanic circulation in the Gulf of Lions under wind conditions influenced by the continental orography (FETCH experiment). *J Geophys Res* 108(C3):8059
- Estoumel C, Auclair F, Lux M, Nguyen C, Marsaleix P (2009) "Scale oriented" embedded modeling of the North-Western Mediterranean in the frame of MFSTEP. *Ocean Sci* 5(2):73–90
- Fennel W, Lass H (2007) On the impact of wind curls on coastal currents. *J Mar Syst* 68:128–142
- Fischer C, Montmerle T, Berre L, Auger L, Stefanescu SE (2005) An overview of the variational assimilation in the ALADIN/France numerical weather-prediction system. *Q J R Meteorol Soc* 131:3477–3492
- Flexas M, de Madron X, Garcia M, Canals M, Arnau P (2002) Flow variability in the Gulf of Lions during the MATER HFF experiment (March–May 1997). *J Mar Syst* 33:197–214
- Garreau P, Garnier V, Schaefer A (2011) Eddy resolving modelling of the Gulf of Lions and Catalan Sea. *Ocean Dynamics* (in press)
- Gatti J, Petrenko A, Devenon J, Leredde Y, Ulses C (2006) The Rhone river dilution zone present in the northeastern shelf of the Gulf of Lion in December 2003. *Cont Shelf Res* 26:17941805
- Gill AE (1982) *Atmosphere-ocean dynamics*. London: Academic Press, p. 662
- Gill AE (1984) On the behavior of internal waves in the wakes of storms. *J Phys Oceanogr* 14:1129–1151
- Grell JDG, Stauffer D (1993) *A Description of the Fifth-Generation Penn State/NCAR Mesoscale Model (MM5)*. Tech. rep., 398th ed., NCAR Tech. Notes, 117 pp.

- Herrmann MJ, Somot S (2008) Relevance of ERA40 dynamical downscaling for modeling deep convection in the Mediterranean Sea. *Geophysical Research Letters* 35(4)
- Herrmann M, Somot S, Sevault F, Estournel C, Deque M (2008) Modeling the deep convection in the northwestern Mediterranean Sea using an eddy-permitting and an eddy-resolving model: case study of winter 1986–1987. *J Geophys Res-Oceans* 113 (C4)
- Hu ZY, Doglioli AM, Petrenko AA, Marsaleix P, Dekeyser I (2009) Numerical simulations of eddies in the Gulf of Lion. *Ocean Model* 28(4):203–208
- Hua B, Thomasset F (1983) A numerical study of the effects of coastline geometry on wind-induced upwelling in the Gulf of Lions. *J Phys Oceanogr* 13(4):678–694
- Huthnance J (2002) Wind-driven circulation in coastal and marginal seas. *Can J Of Remote Sens* 28:329–339
- Isern-Fontanet J, Font J, Garcia-Ladona E, Emelianov M, Millot C, Taupier-Letage I (2004) Spatial structure of anticyclonic eddies in the Algerian basin (Mediterranean Sea) analyzed using the Okubo-Weiss parameter. *Deep-Sea Res II* 51:3009–3028
- Jin X, Dong C, Kurian J, McWilliams JC, Chelton DB, Li Z (2009) SST–Wind Interactions in coastal upwelling: oceanic simulation with empirical coupling. *J Phys Oceanogr* 39(11):2957–2970
- Jordi A, Wang DP (2009) Mean dynamic topography and eddy kinetic energy in the Mediterranean Sea: comparison between altimetry and a 1/16 degree ocean circulation model. *Ocean Model* 29 (2):137–146
- Lafore J, Stein J, Asencio N, Bougeault P, Ducrocq V, Duron J, Fischer C, Hereil P, Mascart P, Masson V, Pinty J, Redelsperger J, Richard E, de Arellano J (1998) The Meso-NH atmospheric simulation system. Part I: adiabatic formulation and control simulations. *Ann Geophys* 16:90–109
- Langlais C, Barnier B, Molines J, Frauni P, Jacob D, Kotlarski S (2009) Evaluation of a dynamically downscaled atmospheric reanalyse in the prospect of forcing long term simulations of the ocean circulation in the Gulf of Lions. *Ocean Model* 30(4):270–286
- Lazure P, Dumas F (2008) An external-internal mode coupling for a 3D hydrodynamical model for applications at regional scale (MARS). *Adv Water Resour* 31(2):233–250
- Lebeaupin-Brossier CL, Ducrocq V, Giordani H (2009) Effects of the air-sea coupling time frequency on the ocean response during Mediterranean intense events. *Ocean Dyn* 59(4):539–549
- Ludwig W, Meybeck M, Abousamra F (2003) Riverine transport of water, sediments, and pollutants to the Mediterranean Sea. UNEP MAP Technical Report, 141, 111
- Luyten P, De Mulder T (1992) A module representative surface fluxes of momentum and heat. Technical report No 9 MAST-0050-C (Mumm), p. 30
- Masson V, Seity Y (2009) Including atmospheric layers in vegetation and urban offline surface schemes. *J Appl Meteorol Climatol* 48 (7):1377–1397
- McCreary J, Lee H, Enfield D (1989) The response of the coastal ocean to strong offshore winds—with application to circulations in the gulf-of-Tehuantepec and Papagayo. *J Mar Res* 47(1):81–109
- Millot C (1979) Wind induced upwellings in the Gulf of Lions. *Oceanol Acta* 2:261–274
- Millot C (1990) The Gulf of Lions' hydrodynamics. *Cont Shelf Res* 10(9–11):885–894
- Millot C (1999) Circulation in the Western Mediterranean Sea. *J Mar Syst* 20(1–4):423–442
- Millot C, Crepon M (1981) Inertial oscillations on the continental shelf of the Gulf of Lions—observations and theory. *J Phys Oceanogr* 11(5):639–657
- Millot C, Wald L (1980) The effect of Mistral wind on the Ligurian current near Provence. *Oceanol Acta* 3:399–402
- Nicolle A, Garreau P, Liorzou B (2009) Modelling for anchovy recruitment studies in the Gulf of Lions (Western Mediterranean Sea). *Ocean Dyn* 59:953–968
- Pacanowski R, Philander S (1981) Parametrization of vertical mixing in numerical-model of tropical oceans. *J Phys Oceanogr* 11:1443–1451
- Petrenko A (2003) Variability of circulation features in the Gulf of Lions NW Mediterranean Sea: importance of inertial current. *Oceanol Acta* 26:323–338
- Petrenko A, Leredde Y, Marsaleix P (2005) Circulation in a stratified and wind-forced Gulf of Lions, NW Mediterranean Sea: in situ and modelling data. *Cont Shelf Res* 25:7–27
- Petrenko A, Dufau C, Estournel C (2008) Barotropic eastward currents in the western Gulf of Lion, north-western Mediterranean Sea, during stratified conditions. *J Mar Syst* 74:406–428
- Pickett M, Paduan J (2003) Ekman transport and pumping in the California Current based on the U.S. Navy's high-resolution atmospheric model (COAMPS). *J Geophys Res Oceans* 108 (10):3327
- Pinardi N, Allen I, Demirov E, De Mey P, Korres G, Lascaratos A, Le Traon PY, Maillard C, Manzella G, Tziavos C (2003) The Mediterranean ocean forecasting system: first phase of implementation (1998–2001). *Ann Geophys* 21:3–20
- Pujol M, Larnicol G (2005) Mediterranean sea eddy kinetic energy variability from 11 years of altimetric data. *J Mar Syst* 58 (3–4):121–142
- Rousset C, Houssais MN, Chassignet EP (2009) A multi-model study of the restratification phase in an idealized convection basin. *Ocean Model* 26:115–133
- Rubio A, Arnau P, Espino M, Flexas M, Jorda G, Salat J, Puigdefabregas J, Arcilla A (2005) A field study of the behaviour of an anticyclonic eddy on the Catalan continental shelf (NW Mediterranean). *Prog Oceanogr* 66(2–4):142–156
- Rubio A, Barnier B, Jorda G, Espino M, Marsaleix P (2009a) Origin and dynamics of mesoscale eddies in the Catalan Sea (NW Mediterranean): insight from a numerical model study. *J Geophys Res Oceans* 114:C06009
- Rubio A, Taillandier V, Garreau P (2009b) Reconstruction of the Mediterranean northern current variability and associated cross-shelf transport in the Gulf of Lions from satellite-tracked drifters and model outputs. *J Mar Syst* 78:S63–S78
- Ruti P, Marullo S, D'Ortenzio F, Tremant M (2008) Comparison of analyzed and measured wind speeds in the perspective of oceanic simulations over the Mediterranean basin: analyses, QuikSCAT and buoy data. *J Mar Syst* 70:33–48
- Seity Y, Brousseau P, Malardel S, Hello G, Bénard P, Bouttier F, Lac C, Masson V (2011) The AROME-France convective scale operational model. *Mon Wea Rev* 139:976–991
- Simpson J, Bowers D (1981) Models of stratification and frontal movement in shelf seas. *Deep Sea Res A* 28(7):727–738
- Smagorinsky J (1963) General circulation experiments with the primitive equation. I. The basic experiment. *Mon Weather Rev* 111:99–165
- Tintore J, Wang D, Garcia E, Viudez A (1995) Near-inertial motions in the coastal ocean. *J Mar Syst* 6(4):301–312
- Tonani M, Pinardi N, Fratianni C, Pistoia J, Dobricic S, Pensieri S, de Alfonso M, et Nittis K (2009) Mediterranean Forecasting System: forecast and analysis assessment through skill scores. *Ocean Sci* 5(4):649–660
- Trasvina A, Barton ED (2008) Summer circulation in the Mexican tropical Pacific. *Deep Sea Res I* 55(5):587–607
- Trasvina A, Ortiz-Figueroa M, Herrera H, Cosio M, Gonzalez E (2003) 'Santa Ana' winds and upwelling filaments of Northern Baja California. *Dyn Atmos Oceans* 37(2):113–129
- Trasviña A, Barton E, Brown J, Velez H, Kosro P, Smith R (1995) Offshore wind forcing in the Gulf of Tehuantepec, Mexico: the asymmetric circulation. *J Geophys Res* 100(10):20649–20663

- Ulses C, Grenz C, Marsaleix P, Schaaf E, Estournel C, Meule S, Pinazo C (2005) Circulation in a semi-enclosed bay under influence of strong freshwater input. *J Mar Syst* 56:113–132
- Ulses C, Estournel C, Bonnin J, de Madron XD, Marsaleix P (2008) Impact of storms and dense water cascading on shelf-slope exchanges in the Gulf of Lion (NW Mediterranean). *J Geophys Res-Oceans* 113(C2)
- Yoshida S, Qiu B, Hacker P (2010) Wind-generated eddy characteristics in the lee of the island of Hawaii. *J Geophys Res Oceans* 115:C03019